P-07-235

Forsmark site investigation

Detection of potential borehole breakouts in boreholes KFM01A and KFM01B

Daniel Ask, Vattenfall Power Consultant AB

Maria V S Ask, Luleå University of Technology

December 2007

Svensk Kärnbränslehantering AB
Swedish Nuclear Fuel
and Waste Management Co
Box 250, SE-101 24 Stockholm
Tel +46 8 459 84 00

ISSN 1651-4416
SKB P-07-235

Forsmark site investigation

Detection of potential borehole breakouts in boreholes KFM01A and KFM01B

Daniel Ask, Vattenfall Power Consultant AB

Maria V S Ask, Luleå University of Technology

December 2007

Keywords: In situ stress orientation, Borehole breakouts, Borehole televiewer, Borehole image processing system.

Summary

In this report a pilot study is presented of the theoretical requirements needed for stress induced spalling to occur in boreholes within the Forsmark site investigation area as well as of the identification of such spalling in two core drilled boreholes, KFM01A and KFM01B, situated in the area. The study was completed in April 2006 and refers to data from the Forsmark site investigation available prior to that time.

Borehole breakouts are formed in the direction of the least horizontal stress when the stress concentration of the in situ stress field around the borehole exceeds the rock strength of the borehole wall. Hence, the orientation of the maximum horizontal stress is 90° off. The theoretical considerations start from an extensive literature exposition, whereas the analyses of borehole breakouts in the two mentioned boreholes have been based on two routinely collected geophysical logging data sets, BoreHole TeleViewer (BHTV) and Borehole Image Processing System (BIPS).

The most essential objective of this report was to investigate if borehole breakouts exist at the Forsmark pre-investigation site. Should breakouts be identified, a secondary objective was to roughly estimate the total length of breakouts and their orientation, i.e. the orientation of minimum horizontal stress, and to correlate the borehole breakouts with existing structures in the boreholes (fractures and fractures zones), as determined by the Boremap mapping (integrated geological mapping of drill cores and colour-TV-images of the borehole wall). A third aim with the study was to relate identified breakouts with the prevailing stress field at Forsmark based on stress measurements performed in boreholes KFM01A, 01B, 02A and 04A. We emphasize that a full characterization of identified breakouts (orientation and magnitude of horizontal stresses) was outside the scope of this report, but may be undertaken at a later stage if borehole breakouts are found. Other objectives of this report were to identify tools and data sets that are required for the full characterization of borehole breakouts and to assess the impact of the drilling process on the origin of borehole breakouts.

This initial analysis of the BHTV and BIPS logs reveals that borehole breakouts have been formed in both boreholes KFM01A and KFM01B. In total, borehole breakouts occur over about 30% of the length of borehole KFM01A (from 112 to 1,001 m borehole length (mbl)) and almost 40% of the length of borehole KFM01B (from 114 to 499 mbl). The initial results suggest that the minimum and maximum horizontal stresses, σ_h and σ_H, are oriented NE-SW and NW-SE, respectively, over most parts of the investigated depth intervals.

Two main types of borehole breakouts have been found: (1) well-developed, deep borehole breakouts that are easy to detect in both BHTV and BIPS logs; and (2) borehole breakouts with small failure depths that are mostly undetectable in BIPS data but clearly revealed in the BHTV amplitude log and to some extent in cross section plots of the borehole geometry. The results of the more “in depth” analysis of selected breakouts in borehole KFM01B indicate that the observed breakout widths of up to 90° can be predicted from the stress profiles presented in /Ask 2007/. However, the stress magnitudes necessary to initiate breakouts cannot be explained for shallow depths by the various stress profiles derived by /Ask 2007/. These profiles indicate that crack initiation does not start until at 300 mvd (metres vertical depth), which may be interpreted as that breakouts with limited failure depth represent initial stages of breakout formation that progressively would grow in depth with time. We suspect that the well-developed breakouts are located in high-stress zones and/or zones with reduced compressive strength, often related to geological features such as fractures. It should also be noted that minor modifications in the stress profile by /Ask 2007/ change the results drastically. Furthermore, pore pressure, which according to /Zoback et al. 1985/ has a pronounced effect on the breakout development, was not considered in the analysis.

Finally, but perhaps most importantly, the drilling process seems to affect the breakout formation. The smaller breakouts, which represent grain-size fallouts in two diametrically opposite sides of the borehole, seem to increase with increasing wear on the drill bit. When the drill bit is exchanged, these fallouts no longer develop. Hence, temperature and possibly feeding force may be factors that need to be considered in order to explain their development. To our knowledge, this has not been reported previously. Further studies are consequently needed in order to fully explain the observed breakouts.

In the upper section of borehole KFM01B, from 50 to 380 mbl, two zones with diametrically opposed pairs of narrow and wiggling fractures were observed in the azimuth image of the BHTV log. These fractures resemble drilling-induced fractures (DIFs), and their orientations agree well with those of the revealed borehole breakouts. Further studies are needed to determine if they are DIFs or not.

In addition to stress-induced borehole elongations, also numerous drilling-induced borehole elongations, i.e. enlargements of the borehole diameter, including washouts, key seats, and various types of grinding marks and drill-bit grooves were observed.

We recommend that a full characterization of the observed breakouts in boreholes KFM01A and KFM01B is conducted. Because stress magnitude determinations based on borehole breakouts, disregarding if calculations are founded on breakout widths and/or depths, are not particularly accurate, we emphasize that the breakout method should focus primarily on the orientations of the stress field. As such, it is extremely valuable, because continuous information along a borehole is collected, which can be used to pinpoint decoupling zones in the rock; zones that seldom can be identified using point-wise measurements. Hence, we consider studies of borehole breakouts in the Forsmark area as one of the most important targets in the rock mechanical part of the ongoing site investigation program (see further Chapter 7).

Sammanfattning

I denna rapport presenteras en pilotstudie av dels de teoretiska förutsättningarna för spänningsinducerade utfall (på engelska ”borehole breakouts”) i borrhål i Forsmarks platsundersökningsområde, dels identifiering av sådana utfall i två kärnborrhål, KFM01A och KFM01B, belägna inom undersökningsområdet. Utfallen sammanfaller med riktningen av den minsta horisontalspänningen och uppstår när spänningskoncentrationen kring hålet överstiger bergets hållfasthet. Den teoretiska studien bygger på en omfattande litteraturgenomgång, medan analysen av spänningsinducerade utfall i KFM01A och KFM01B har baserats på två rutinmässigt insamlade typer av loggingdata: akustisk BoreHole TeleViewer (BHTV) och Borehole Image Processing System (BIPS).

Det viktigaste målet med studien var att undersöka om utfall ur borrhålsväggen förekommer i borrhål i Forsmarksområdet. Om utfall kunde identifieras, var ett sekundärt mål med studien att grovt uppskatta deras längd och orientering samt att korrelera utfallen med existerande Boremapkarterade (integrerad geologisk kartering av borrkärnor och färg-TV-bilder av borrhålsväggen) strukturer i borrhålen, i första hand enskilda sprickor och sprickzoner, samt att relatera dessa utfall till det rådande spänningsfältet baserat på mätningar i kärnborrhålen KFM01A, 01B, 02A och 04A. Vi vill understryka att en fullständig karakterisering av eventuella utfall, dvs detaljerad uppskattning av orientering och bedömning av magnituder, inte ingick i studien. Detta är i stället ämnat för en eventuell senare aktivitet. Andra syften med studien var att identifiera verktyg och data som krävs för karakterisering av utfallen liksom att undersöka borrningsprocessens eventuella påverkan på uppkomsten av utfall.

Studien visar entydigt att spänningsinducerade utfall har uppkommit i de två studerade Forsmarksborrhålen. Utfall identifierades mellan 112 och 1 001 m borrhålslängd (mbl) i borrhål KFM01A och mellan 114 och 499 mbl i borrhål KFM01B och omfattar därmed ca 30–40 % av den totala borrhålslängden. En preliminär analys ger vid handen att minsta och största huvudspänning, σ_h och σ_H, är orienterade NO-SV respektive NV-SO över de flesta av de borrhålsintervall som undersökts.

Två huvudtyper av utfall upptäcktes: (1) fullt utbildade, djupa utfall som identifierades med både BHTV- och BIPS-data; och (2) utfall med begränsat djup och som generellt enbart kunde identifieras med BHTV. Resultaten från en fördjupad analys av vissa utvalda utfall visade att den observerade utfallsvidden om ca 90° kan förklaras med den relativt grova, preliminära spänningsprofilen från /Ask 2007/ som baseras på hydrauliska data. Däremot kan inte de spänningsmagnituder som krävs för att utfall skall uppstå härledas för grunda djup från de olika spänningsprofiler som /Ask 2007/ tagit fram. Spänningsprofilerna indikerar att sprickinitiering påbörjas först vid ca 300 m vertikaldjup, vilket skulle kunna tolkas som att utfallen med begränsat djup inte är fullt utbildade, utan riskerar att fördjupas med tiden. Vår tolkning av de djupa och fullt utbildade utfallen är att de sammanfaller med sektioner med förhöjda spänningsnivåer och/eller reducerad hållfasthet. Vi vill betona att små förändringar i de av /Ask 2007/ framtagna spänningsprofilerna förändrar resultaten drastiskt, samt att portryckseffekter, som enligt /Zoback et al. 1985/ kan ha en betydande inverkan på bildandet av spänningsinducerade utfall, inte har beaktats i de utförda analyserna.

Slutligen bör framhållas att borrningsprocessen tycks påverka bildandet av utfall med begränsat djup, speciellt utfall i kornstorleksnivå. Dessa uppträder tydligast i samband med att borrkronan börjar slitas för att helt försvinna i samband med byte av borrkrona. Detta indikerar att temperatur och eventuellt matningstryck påverkar bildandet, något som så vitt oss är bekant inte lyfts fram i litteraturen tidigare. Vi förordar därför fortsatta studier av borrningens effekt på utfall i borrhål.

Både BHTV och BIPS indikerar ett relativt stort antal existerande sprickor och sprickzoner, vilka ofta sammanfaller med någon form av utfall. Potentiella borrinducerade dragsprickor påträffades i borrhål KFM01B, men en ytterligare analys krävs för verifiering. Slutligen påvisar både BHTV och BIPS omfattande borrinducerad mekanisk påverkan på borrhålsväggen.

Vi rekommenderar att en mer fullständig karakterisering av de observerade utfallen i borrhål KFM01A och KFM01B utförs. Eftersom metoden endast ger relativt grova uppskattningar av spänningsmagnituder bör fokus ligga på orienteringen av spänningarna. I det syftet är metoden unik och mycket värdefull, eftersom kontinuerlig information erhålls som kan användas för att identifiera geologiska diskontinuiteter som påverkar spänningsfältet. Sådana diskontinuiteter är oftast mycket svåra att upptäcka med punktvisa mätningar med överborrning och hydrauliska metoder. Vi anser därför att studier av utfall i borrhål utgör ett mycket viktigt område inom den bergmekaniska delen av det pågående platsundersökningsprogrammet (se vidare kapitel 7).

Contents

1 Introduction

This report presents results from a multi-purpose pilot study of borehole breakouts in the crystalline environment of the Forsmark site investigation area, Sweden. This is part of the site investigation programme managed by Swedish Nuclear Fuel and Waste Management Co (SKB). Besides theoretical considerations, the activity focused on, with aid of two borehole geophysical logging methods, identifying borehole breakouts in two core drilled boreholes, KFM01A and KFM01B, situated within the north-western part of the so called Forsmark candidate area, see Figure 1-1. These boreholes, which were recommended by SKB, are c 1,000 and 500 m long, respectively. Their inclinations at ground surface with respect to the horizontal are 85° and 79°.

Figure 1-1. *The Forsmark investigation area with all boreholes in which overcoring and hydraulic rock stress measurements have been conducted up to April 2006. Boreholes KFM01A and KFM01B are located in the north-western part of the candidate area.*

Normally, site investigations managed by SKB are performed in compliance with internal SKB controlling documents of two kinds: activity plans and method documents (the latter consisting of method descriptions, method instructions and descriptions of measurement systems). Regarding the present activity, there exist no SKB method documents, and the activity was not aiming at providing data to be stored in SKB's databases. SKB's instructions to the Contractor were presented during a meeting at the SKB Stockholm head office 2004-10-18 (participants: Activity Leader Rolf Christiansson, SKB, professor Derek Martin, University of Alberta, Canada (SKB representative) and Dr Daniel Ask, Vattenfall Power Consultant (Contractor representative)). The meeting was followed by e-mail correspondence with additional instructions and the work started 2005-05-13. The study was completed in April 2006 and refers to data from the Forsmark site investigation available prior to that time. Several references in this report concern /Ask 2007/, which presents results from a study performed 2004–2005, although the report was not printed until 2007.

Currently (2006), five types of stress measuring methods, direct and indirect, have been applied and analyzed at the Forsmark site: (1) overcoring /Sjöberg 2004, Lindfors et al. 2004, Ask 2007/; (2) hydraulic fracturing /Klee and Rummel 2004, Ask 2007/; (3) hydraulic tests on pre-existing fractures /Klee and Rummel 2004, Ask 2007/; (4) core discing /Lindfors et al. 2004, Sjöberg et al. 2005/; and (5) spalling failures /Lindfors et al. 2004, Sjöberg et al. 2005/. These methods generally provide point-wise estimates of local stress tensors that usually probe a small section of a borehole. The regional stress tensor is obtained from successive rock stress measurements of local stress tensors.

The borehole breakout method is an important indicator of horizontal stress orientation, particularly in aseismic regions and at small and intermediate depths (< 5 km). Borehole breakouts are stress-induced borehole elongations that commonly appear over large sections along a borehole. As a result, borehole breakouts may provide continuous information on the state of stress, and therefore reveal important information on the continuity of the stress field in the rock mass. Borehole breakouts are formed in borehole sections where the stress concentration at the borehole wall exceeds the strength of the rock. It is well known that borehole breakouts are formed parallel to the direction of minimum horizontal stress, σ_h, because maximum stress concentration is built up at the borehole wall in this direction /e.g. Bell and Gough 1979/. Until now, the borehole breakout method has not been applied to any of the SKB investigation sites.

Borehole breakouts can be detected using standard geophysical logging tools that map the geometry of the borehole wall. As a result, this method is less expensive in comparison to most other stress measuring methods. The SKB standard logging data include the acoustic Borehole Televiewer (BHTV) and the optical and digital Borehole Image Processing System (BIPS). The BHTV tool provides two types of velocity images of the borehole wall, whereas the BIPS tool provides a digital video image of the borehole wall. In standard application, BIPS data are used for describing the lithology and structural geology of the boreholes, and for reorienting drill cores. BHTV data are primarily used for describing the geometry of the borehole wall, and this knowledge is important for environmental corrections as borehole size and roughness may partially mask or disrupt the log response from the formation for other types of geophysical logging data. In this report, we use the velocity images from the BHTV and the digital images of the BIPS tools to detect stress- and drilling-induced borehole elongations. These data provide information on the state of stress, and the analyses involve characterization of borehole breakouts, determination of location, size, and orientation of fractures intersecting the borehole, and detection of slips on reactivated faults.

Throughout this report, stresses are denoted using a geomechanical sign convention with compressive stresses taken as positive. Stress orientations are given with respect to geographic North according to coordinate system RT90, 2.5 gon W 0:-15, using a right-hand rule notation. The work presented is one of the activities within the site investigations at Forsmark.

2 Objective and scope

The primary objectives and scope of this report were 1) to perform a theoretical survey of the general requirements for the occurrence of borehole breakouts in the kind of crystalline environment and with the stress field prevailing at Forsmark, 2) to test two methods to detect borehole breakouts of macro- as well as of micro-scale, 3) to try to identify the possible existence of borehole breakouts in two boreholes (KFM01A and KFM01B) situated within the north-western part of the Forsmark candidate area, and 4) to study the impact of the drilling process on the origin of borehole breakouts.

The positive identification of numerous shallow and some deeper breakouts has lead to the additional objectives to: 5) make a preliminary assessment of the extent of borehole breakout occurrence in the two mentioned boreholes, and 6) roughly estimate their orientation that reveals the minimum principal horizontal stress. It is, however, not the scope of this report to make a detailed study of borehole breakout occurrence and characterization of the state of stress (orientation and magnitude). However, because two types of breakouts were found, shallow and deeper, a thorough analysis of a couple of selected borehole breakout sections in borehole KFM01B was performed.

The final objective of this study was to 7) give recommendations for required data and tools for a future detailed study of borehole breakout occurrence and characterization of the state of stress in boreholes KFM01A and KFM01B.

3 Borehole breakout theory, measurement and analyses

3.1 General

Borehole breakouts are stress-induced enlargements of the borehole cross section /Bell and Gough 1979/. They appear when the stress concentration around the borehole exceeds the rock strength /e.g. Zoback et al. 1985/. The breakouts form on diametrically opposite sides of the borehole, are parallel to the minimum horizontal stress (σ_h), and generally vary in length from less than a metre to several tens of metres /Bell and Gough 1979/ (Figure 3-1).

The borehole breakout method has since the late 1970s commonly been applied for determination of in situ stress orientations, because its analysis is based on data from standard logging tools /e.g. Bell and Gough 1979/. For example, about 20% of the data in the World Stress Map (WSM) are borehole breakout data /Reinecker et al. 2004/.

3.2 Theory

Breakout theory was originally proposed by /Bell and Gough 1979/ and /Gough and Bell 1981/, based on the equations of /Kirsch 1898/. Since then others have expanded the theory and interpretation to: (1) include effective stresses and account for the effect of the difference in pressure between the drilling fluid and the rock formation /Zoback et al. 1985/; (2) analyze data from inclined boreholes /e.g. Mastin 1988, Peska and Zoback 1995, Zajac and Stock 1997/; (3) estimate the stress regime from the breakout depth distribution /Moos and Zoback 1990/; (4) estimate principal stress magnitudes from breakout shape /Zoback et al. 1985, Barton et al. 1988, Zheng et al. 1988, Peska and Zoback 1995, Zajac and Stock 1997/; and (5) study fracture initiation and other types of borehole failure /Guenot 1987, Plumb 1989, Moos and Zoback 1990, Haimson and Song 1993/. In addition, a state of the art paper has recently been published by /Zoback et al. 2003/, in which existing theories are summarized.

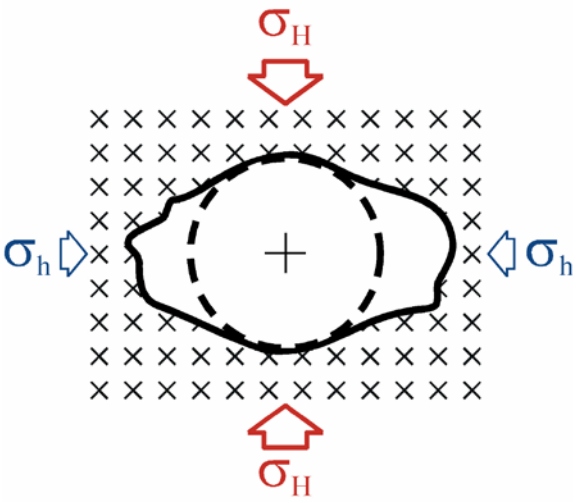

Figure 3-1. *Graphical presentation of stress-induced borehole breakout (modified after /Ask 1998/).*

The stress concentration around a (near-) vertical borehole in a horizontal plate includes radial, circumferential and shear stresses. The plate is assumed composed of an ideally elastic and isotropic material with one of the principal stresses in the direction of the borehole, and subjected to a homogeneous stress field. The theoretical relationship for applied far-field stresses was first described by /Kirsch 1898/ and subsequently by others /e.g. Jaeger and Cook 1969/:

$$\sigma_r = \frac{(\sigma_H + \sigma_h)}{2} \cdot \left(1 - \frac{R^2}{r^2}\right) + \frac{(\sigma_H - \sigma_h)}{2} \cdot \left(1 - 4 \cdot \frac{R^2}{r^2} + 3 \cdot \frac{R^4}{r^4}\right) \cdot \cos 2\theta + \Delta P \cdot \frac{R^2}{r^2} \quad (1)$$

$$\sigma_\theta = \frac{(\sigma_H + \sigma_h)}{2} \cdot \left(1 + \frac{R^2}{r^2}\right) - \frac{(\sigma_H - \sigma_h)}{2} \cdot \left(1 + 3 \cdot \frac{R^4}{r^4}\right) \cdot \cos 2\theta - \Delta P \cdot \frac{R^2}{r^2} \quad (2)$$

$$\tau_{r\theta} = -\frac{(\sigma_H + \sigma_h)}{2} \cdot \left(1 + 2 \cdot \frac{R^2}{r^2} - 3 \cdot \frac{R^4}{r^4}\right) \cdot \sin 2\theta \quad (3)$$

where σ_H and σ_h are the maximum and minimum horizontal stresses, R is the borehole radius, r the radial distance to the measurement point, θ is the angle from σ_H, ΔP is difference between the borehole fluid pressure, P_b, and the formation pore pressure, P_o. Note that these equations are subject to the hypothesis of fluid percolation (in case fluid percolation is absent, the term $\Delta P \cdot R^2/r^2$ is reduced to ΔP in Equations (1) and (2)).

At the borehole wall, $r = R$, and the formulas reduce to:

$$\sigma_r = \Delta P \quad (4)$$

$$\sigma_\theta = (\sigma_H + \sigma_h) - 2 \cdot (\sigma_H - \sigma_h) \cdot \cos 2\theta - \Delta P \quad (5)$$

$$\tau_{r\theta} = 0 \quad (6)$$

where $\Delta P = P_b - P_0$.

Maximum stress concentration occurs at $\theta = 0°$, which is the direction of borehole breakout formation. Minimum stress concentration occurs at $\theta = 90°$, which is the direction of hydraulic fracturing formation. For the borehole breakout case, Equation (5) reduces into Equation (7). Correspondingly, Equation (5) reduces into Equation (8) for the hydraulic fracturing case:

$$\sigma_{\theta=90°} = 3 \cdot \sigma_h - \sigma_H - \Delta P \quad (7)$$

$$\sigma_{\theta=0°} = 3 \cdot \sigma_H - \sigma_h - \Delta P \quad (8)$$

The specific failure mechanisms of borehole breakouts may vary with rock strength, depth, and state of stress /Plumb 1989/. Detailed observations of breakouts in several stages of development suggest that borehole failure is dependent on lithology /Plumb 1989/. He observed that breakouts in crystalline rocks are small pits at the borehole wall, whereas breakouts first appear as well-developed diametrical fractured sections in sedimentary rocks. From these observations, /Plumb 1989/ suggests that breakout failure in crystalline rocks initiates at the borehole wall, whereas it initiates inside the formation in sedimentary rocks. From compilation of breakout images, /Plumb 1989/ presents three main types of breakouts, which reflect one of three reference states of stress around the borehole: Type 1 forms at a stress state of $\sigma_r < \sigma_z < \sigma_\theta$, and consists of vertical fractures parallel to the borehole; Type 2 is formed when $\sigma_r < \sigma_\theta < \sigma_z$, and consists of horizontal extension fractures with shear fractures at a sharp angle to the borehole wall; and Type 3 is formed when $\sigma_\theta < \sigma_r < \sigma_z$, and consists of stepped fractures developed from inclined fractures.

By considering rock anisotropy and state of stress, /Maury et al. 1999/ suggest that six theoretical rupture modes occur at compressional stress states in boreholes that are sub-aligned to one principal stress direction: A1, A2, B1, B2, C1 and C2 (Figure 3-2). Each of the shear modes may appear on the whole periphery or part of the borehole periphery, according to the presence of a laterally isotropic or anisotropic stress field. Corresponding caving shapes are indicated on

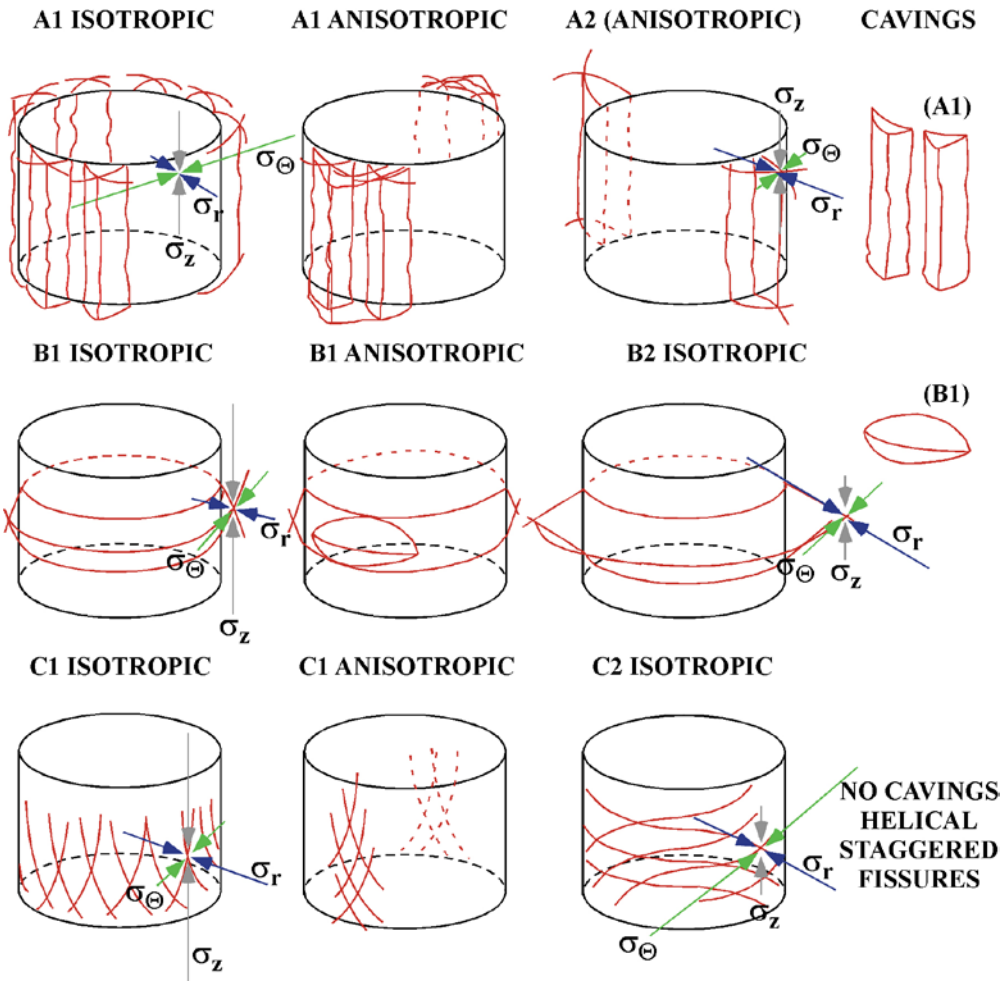

Figure 3-2. *Shear rupture modes around a (vertical) borehole /after Maury et al. 1999/. Length of arrow is proportional to stress magnitude. Green arrow, σ_θ; blue arrow, σ_r; grey arrow, σ_z.*

the right-hand side of Figure 3-2. The A1 and A2 rupture modes correspond to the well-known "borehole breakouts", for which the horizontal (tangential) stress at the borehole wall exceeds the compressional strength of the rock (the axial stress is the intermediate stress). The B1 and B2 modes are a result of excess of vertical stress relatively to the internal pressure (tangential stress is intermediate). The C1 and C2 rupture modes involve excessive internal pressure relatively to external stress and are believed as feasible due to the accommodation of elastic deformation in the unruptured parts of borehole but do not produce cavings (radial stress is intermediate; /Maury et al. 1999/).

/Maury et al. 1999/ also propose possible modes of rupture in extension and traction (Figure 3-3). The extension mode E (isotropic or anisotropic) corresponds to similar conditions as for the compression mode A1, with $\sigma_r < \sigma_z < \sigma_\theta$ (here $\sigma_r \approx 0$ and the rock behaviour is very brittle).

The vertical (D1) and horizontal (D2) true traction modes (hydraulic fracturing) are well known, and traction mode D3 is induced by tensile radial stress inside the wall ($\sigma_r \approx 0$). The latter has been observed as developing in cores. The three modes A1, E1, and D3 (radial stress) are often differentiated for identification purpose.

More comprehensive discussions on the theory of breakout formation are given by e.g. /Engelder 1993/ and /Amadei and Stephansson 1997/.

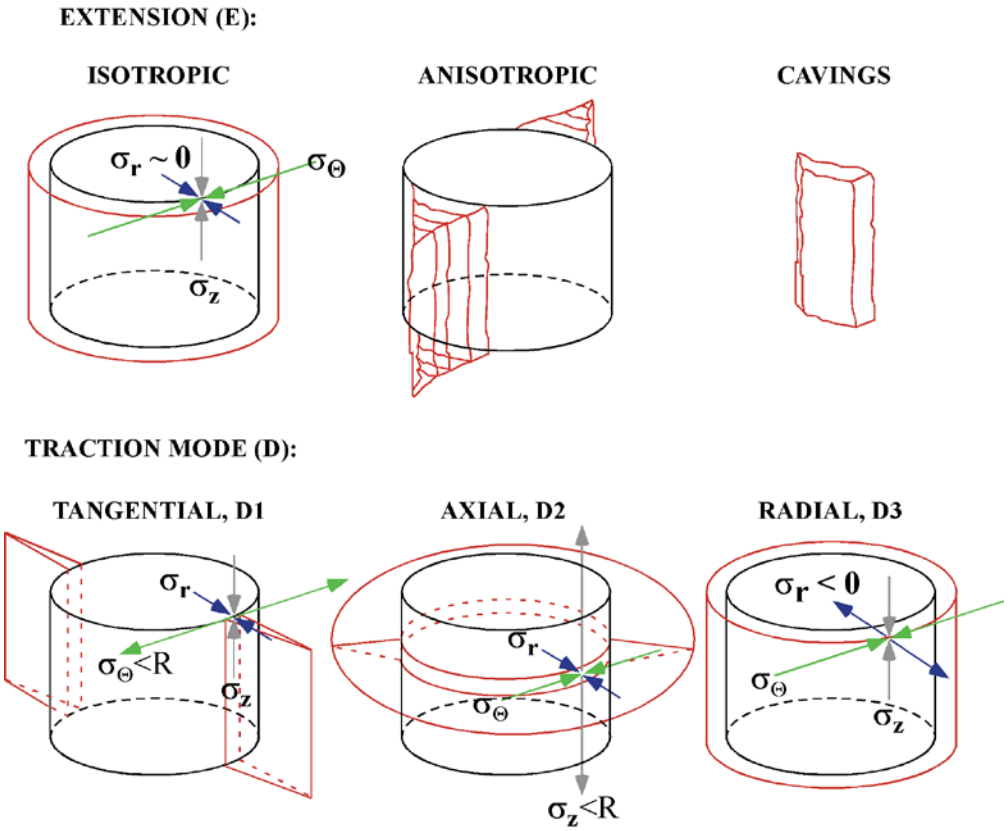

Figure 3-3. *Extension and true traction rupture mode in a (vertical) borehole /after Maury et al. 1999/. Length of arrow is proportional to stress magnitude. Green arrow, σ_θ; blue arrow, σ_r; grey arrow, σ_z.*

3.3 Measurement

Borehole breakouts are commonly identified using standard logging tools such as oriented four-arm caliper, borehole televiewer (BHTV), and Formation MicroScanner (FMS). The four-arm caliper tool provides measurement of the borehole geometry in two orthogonal directions, as well as the position of the tool with respect to magnetic North and vertical. The BHTV tool collects two types of detailed acoustic data (travel time and amplitude images) of the borehole wall that provide information on the borehole diameter and acoustic impedance. These images can be used to detect borehole breakouts, DIFs (drilling-induced fractures), and other structures that have an acoustic contrast to the borehole wall (Figure 3-4).

Several different borehole geometries may be encountered during analyses. At good conditions (i.e. centralized tool, clear borehole fluid, and sufficient acoustic contrast at the borehole wall), BHTV images provide a detailed shape of the borehole wall that allows separation between drilling- and stress-induced (key seats, washouts, borehole breakouts, DIFs) borehole elongations (Figure 3-5). The FMS tool collects both conventional four-arm caliper data (for breakout analyses) and small-scale conductivity images (for analyses of DIFs).

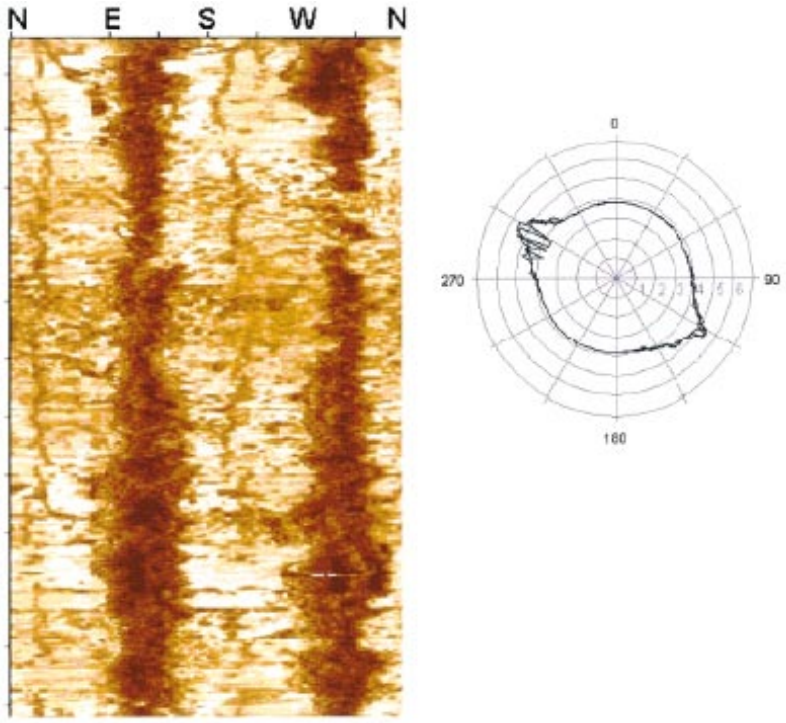

Figure 3-4. *Example of borehole breakouts. In the BHTV amplitude image (left), the borehole breakouts appear as dark, wide bands (low reflection amplitudes), 180° apart. Note also the existence of drilling-induced fractures 90° from the breakouts. Cross sections of the borehole (right) allow clear identification of borehole breakouts /from Zoback et al. 2003/.*

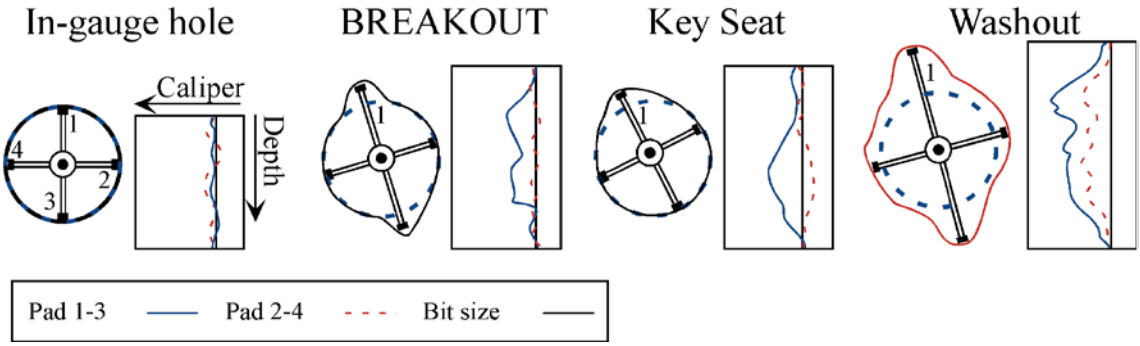

Figure 3-5. *Examples of common borehole geometries and their expression in four-arm caliper logs (modified after /Plumb and Hickman 1985/).*

3.4 Analyses

/Plumb and Hickman 1985/ compared BHTV and four arm-caliper data. Their study entailed identification of four common borehole geometries /Plumb and Hickman 1985/ (Figure 3-5): (1) an in-gauge hole that has dimensions of the drill bit; (2) a breakout has one diameter elongated but the orthogonal diameter remains at the original bit size; (3) a key seat occurs when the drill-string wear has caused a pear-shaped borehole. The risk for key seats, or drill-pipe wear, increases with increasing borehole inclination (as well as lengths); and (4) a washout appears as an increase in all dimensions of the borehole.

The limitation of the BHTV tool is associated with the fact that the tool emits and receives ultrasonic pulses. Particles in the borehole fluid scatter and prevent part of the pulse from reflecting at the borehole wall. The results are depending on acoustic contrasts at the borehole wall. Fractures, voids, soft material, as well as borehole breakouts and drilling-induced fractures (DIFs) absorb or scatter much of the pulse, which produce low-amplitude and high travel time reflectance or dark zones in the unwrapped images. The quality of the results depends on whether or not the tool is centralized in the borehole. /Deltombe and Schepers 2000/ discuss different effects of decentralized tool, and a summary is given in the sections below and in Figure 3-6.

/Deltombe and Schepers 2000/ start the discussion by reaffirming that the BHTV tool measures multiple distances from the tool to the borehole wall, which may not be equal to borehole caliper measurements because caliper is only defined with respect to the centre of a regular shaped borehole. They discussed two scenarios of decentralized tool in an in-gauge (circular) and elongated borehole, respectively (Figure 3-6A). The acoustic beam can hit the borehole wall at perpendicular (green arrows, or beams) and inclined (red arrows or beams) angles. For the case when the tool is decentralized in an in-gauge borehole, the "green" beams provide data on maximum reflection amplitudes and correct travel times. On the other hand, all "red" beams provide measures of secants, and their lengths depend on the position of the tool. For the case when the tool is decentralized in an elongated borehole, neither of the "green" or "red" beams provide meaningful data.

Figure 3-6B shows an example of BHTV data for the case when the tool is decentralized in an in-gauge borehole /Deltombe and Schepers 2000/. The travel time (left image) contains a clear maximum (yellow) and minimum (dark blue). The difference between maximum and minimum is changing versus depth, as well as the direction of maximum and minimum, which suggest that the amount of decentralization and its direction is changing with depth. The travel time image contains little further information about the borehole shape, which implies that the borehole wall is relatively smooth. The middle image shows uncorrected amplitude data, which reveals the influence of decentralization as two broad shades (light brown) running parallel to the variation of the travel time image. The narrow dark brown line in the amplitude images is due to tool construction. The influence of decentralization can be removed to some extent from the amplitude image by a 2D high-pass filter. The result of the process is shown in the rigth image of Figure 3-6B, Amplitude (corrected).

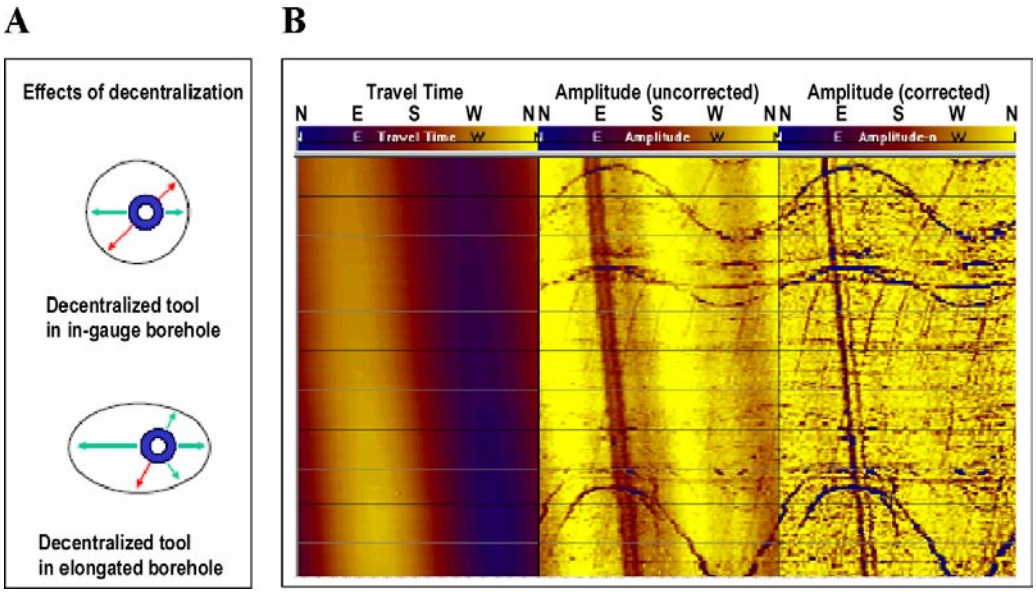

Figure 3-6. *Effects of a decentralized tool. A) Schematic presentation of effects of decentralization. B) BHTV data for a decentralized tool in an in-gauge borehole. See text for discussion (modified from /Deltombe and Schepers 2000/).*

/Deltombe and Schepers 2000/ observe that the widths of amplitude anomalies are larger than those of travel time anomalies (i.e. borehole elongations). They conclude that amplitude images are more sensitive than the travel time images to detect defects in the rock. They argue that the amplitude image detects if some material is already partly destroyed before it is visible on the travel time image. /Deltombe and Schepers 2000/ further propose that the amplitude image can be considered as an additional tool, useful not only to see existing breakouts but also to detect potential breakout areas. They also conclude that their new results call for careful consideration of how the widths of breakouts are determined.

Decentralization can be prevented if centralizer springs are mounted on the BHTV tool. However, the tool can become decentralized even if centralizer springs are in use, because of either or a combination of: the number of centralizer springs and their position on the tool, the borehole diameter with respect to the centralizer springs, and on the dip angle of the borehole.

4 Data

RAMBØLL conducted BHTV measurements in boreholes KFM01A and KFM01B using a centralized High Resolution Acoustic Televiewer from Robertson Geologging Ltd, *RG 25 112 000 HiRAT*. Some specifications of the BHTV tool are given in Table 4-1. The results from logging in boreholes KFM01A and KFM01B are summarized in /Nielsen and Ringgaard 2003, 2004/.

Note that the specifications obtained at the Robertson Geologging Ltd web site differ slightly with specifications by RAMBØLL regarding diameter and lengths of probe, see comment Chapter 7.

The BHTV tool uses a fixed acoustic transducer and rotating mirror system to acquire two-way travel-time and amplitude of the acoustic signal reflected back to the transducer from a spiral trajectory on the borehole-wall. The start of each spiral is referenced to Magnetic North during acquisition, using data from the 3-axis magnetometer-accelerometer unit in the probe. The vertical sampling interval of the spiral trajectory depends on the logging speed and the rotation-rate of the mirror. The speed of logging varied, and was 2.0 m/min in borehole KFM01A and 2.4 m/min in borehole KFM01B /Nielsen and Ringgaard 2003, 2004/. /Nielsen and Ringgaard 2003/ specified that the vertical sampling interval was 2 mm in borehole KFM01A, implying that the maximum transducer frequency of 20 revolutions per second was used during logging. The transducer frequency of 1.5 MHz corresponds to a wavelength of 0.7 µm, but the accuracy is lower than 0.7 µm as a result of the combined effects of logging speed, rotation-rate of the mirror, transducer frequency, as well as of the centralization of tool within the borehole, and on the types of processing that are applied to the data. In a recent study, Håkan Mattsson (pers. comm. 2006) suggests that the radial resolution of the data from boreholes KFM01A and KFM01B is at least ± 0.2 mm.

Six parameters are included in the standard representation of the *RG 25 112 000 HiRAT* data (Figure 4-1):

(1) TRAVEL TIME is a 360° oriented travel time image in grey-scale. Travel-time units are 0.1 µs, and reveals the borehole diameter provided that an estimate of acoustic velocity in the borehole fluid is available.

(2) AMPLITUDE is a 360° oriented amplitude image in colour-scale. Amplitude is dimensionless and reveals the acoustic impedance of the borehole wall that is related to geotechnical rock properties.

(3) AZIMUTH MN is the orientation of the tool with respect to magnetic North (0–360°N). The data have been corrected for the magnetic declination.

(4) DIP is the borehole inclination from the horizontal, which varies from 0–90°. Note that DIP reveals the orientation of the tool within the borehole, which may not follow the orientation of the borehole, because of the smaller probe diameter (45 mm) relative to the borehole diameter (76 mm).

(5) CALIPER 3D is calculated using the acoustic travel time and the velocity in the borehole fluid. The velocity in the fluid is calculated using the fluid temperature and fluid conductivity /Nielsen and Ringgaard 2003, 2004/.

(6) CALIPER MEAN is calculated using the mean travel time from the acoustic televiewer, the fluid temperature, fluid velocity and the internal travel time in the televiewer instrument.

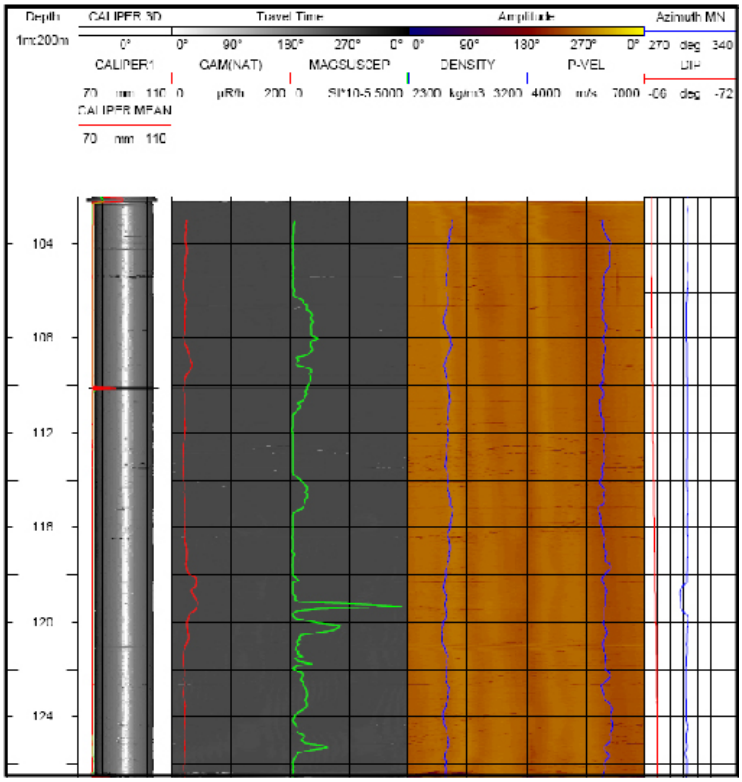

Figure 4-1. *Standard presentation of unwrapped BHTV data from the top of borehole KFM01A, over the depth interval between 102 and 126 mbl (metres borehole length, scale 1:200). The* RG 25 112 000 HiRAT *tool records six parameters, discussed in text above. Note that CALIPER1, GAM(NAT), MAGSUSCEP, DENSITY, and P-VEL are parameters collected by other tools during different runs /from Nielsen and Ringgaard 2003/.*

Table 4-1. Specifications for *RG 25 112 000 HiRAT* (obtained from http://www.geologging.com/index.html)**.**

Probe 25 112 000 HRAT	high resolution acoustic televiewer probe
Diameter	45 mm
Length	1.98 m (including natural-gamma option, probe RG 112 005)
Weight	10 kg
Transducer type	focused piezoelectric
Transducer frequency	1.5 MHz
Transducer rotation rate	5–20 revolutions/second
Firing rate	90/180/270/360 steps/rev (user selectable)
Orientation transducer	3-axis magnetometer, 3-axis accelerometers for true 3D operation

The BIPS method for borehole logging produces an optical, digital scan of the borehole wall (Figure 4-2). A standard CCD video camera is installed in the probe in front of a conical mirror. An acrylic window covers the mirror part, and the borehole image is reflected through the window part and displayed on the cone, from where it is recorded. During measurement, pixel circles are scanned with a resolution of 360 pixels/circle. The BIPS system is described in more detail in the method description “Metodbeskrivning för TV-loggning med BIPS” (SKB MD 222.006, Version 1.0). The system orientates the BIPS images using a compass (vertical boreholes) or with a gravity sensor (inclined boreholes; /Aaltonen and Gustafsson 2003/).

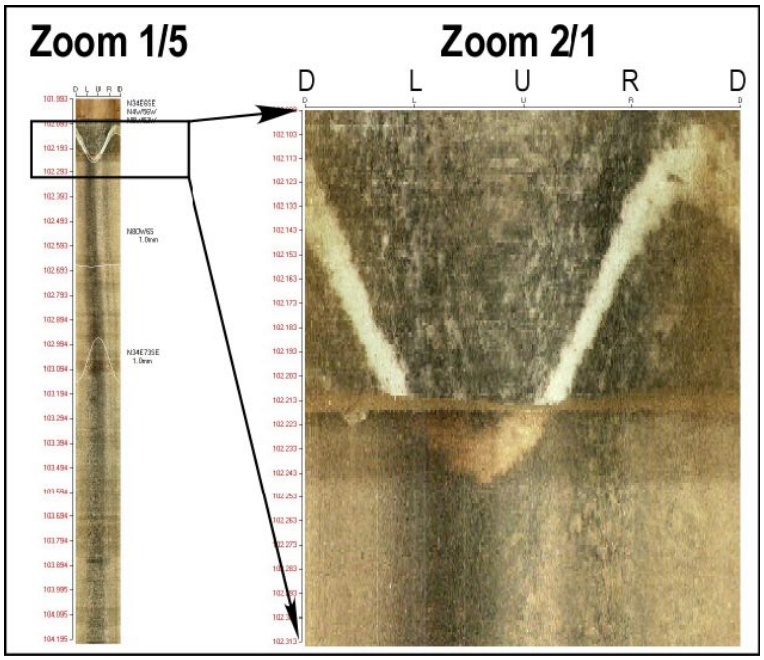

Figure 4-2. *Standard presentation of unwrapped BIPS data from the top of borehole KFM01A. The BIPS data are plotted at maximum (Zoom 1/5) and minimum (Zoom 2/1) scale. Zoom 1/5 is plotted at adjusted depth from 101.993 to 104.195 mbl. Corresponding depths for Zoom 2/1 are 102.093 to 102.313 mbl. BIPS data can be presented either at recorded depth (black text) or adjusted depth (red text). Data interpretation can be included (like in Zoom 1/5) or excluded (like in Zoom 2/1). The BIPS images are oriented with respect to the upper side of the tool, and not with respect to magnetic North: D = downside of tool, L = left side of tool, U = upper side of tool, and R = right side of tool /from Petersson and Wängnerud 2003/.*

The precision of the orientation of the system downhole using a gravity sensor is of the order of 1°, but it is dependent on the operator, who manually records the orientation. Stenberg (pers. comm. 2006) estimated the imprecision in orientations to 2–3° during logging.

Both systems were calibrated against drilled reference grooves in the borehole wall. There is a slight depth difference between the systems, which is discussed in Chapters 6.3 and 7.

SKB provided two computer programs for analyzing the logging data: WellCAD Reader, Version 4.0 build 1008, was used to view BHTV, and BIPS Image Viewer for Windows 95/NT, Version 2.51, was employed for viewing the BIPS data. Table 4-2 summarizes names of the files that are included in this study and provided by SKB from Sicada (delivery Sicada_05_091).

Table 4-2. Name of data files used in this study (delivery Sicada_05_091).

Borehole	Name of data file	Type of data
KFM01A	KFM01A_101-996.BIP	BIPS data including structural interpretation.
	KFM01A_101-996.bdt	
	KFM01A_Presentation_with_SP.WCL	Geophysical logging data including BHTV, Caliper-1, density, P-wave velocity, rock and borehole fluid resistivity, borehole temperature, and natural gamma radiation data.
KFM01B	KFM01B_15-497m_20040415c.BIP	BIPS data including structural interpretation.
	KFM01B_15-497m_20040415c.bdt	
	KFM01B_Presentation.WCL	Geophysical logging data including BHTV, Caliper-1, density, P-wave velocity, rock and borehole fluid resistivity, borehole temperature, and natural gamma radiation data.

The borehole geometry was primarily identified in WellCAD Reader, Version 4.0 build 1008. The amplitude image plotted as function of azimuth and depth were used for initial identification of potential zones of borehole elongations. The detailed view of the borehole geometry was obtained from plotting cross sections of the 3D caliper data using the routine "3D editor" in WellCAD Reader. In this presentation, unwrapped results from the travel time and amplitude logs, as well as individual thin slices of the borehole cross sections are inspected. An understanding of the change in downhole borehole cross section is achieved by stepwise changes in depth of the cross section slices. BIPS Image Viewer proved to be excellent in revealing small-scale fractures; hence it was primarily used for verifying breakouts and/or for inspecting lithologic borders.

Generally, the borehole geometry is best viewed with BHTV data. The cross section borehole geometry is obtained by stacking a 5-mm-long depth interval of CALIPER 3D data (Figure 4-3A). The widths of breakouts, on the other hand, are best viewed on unwrapped amplitude logs (Figure 4-3B). This is especially true for the breakout with small failure depth. In some instants, BIPS images clearly reveal borehole breakouts: (1) Rugged borehole breakouts and fractures are easily identified, especially at smaller scale (or zoom) (Figure 4-2); and (2) Smooth, shallow borehole breakouts may be detected if they occur in dark rocks, because the pits from fall-out grains produce reflecting bands in darker rock types (discussed in Chapter 5).

We emphasize that the careful analyzes of travel time and amplitude logs as suggested by /Deltombe and Schepers 2000/ is outside the scope of this study.

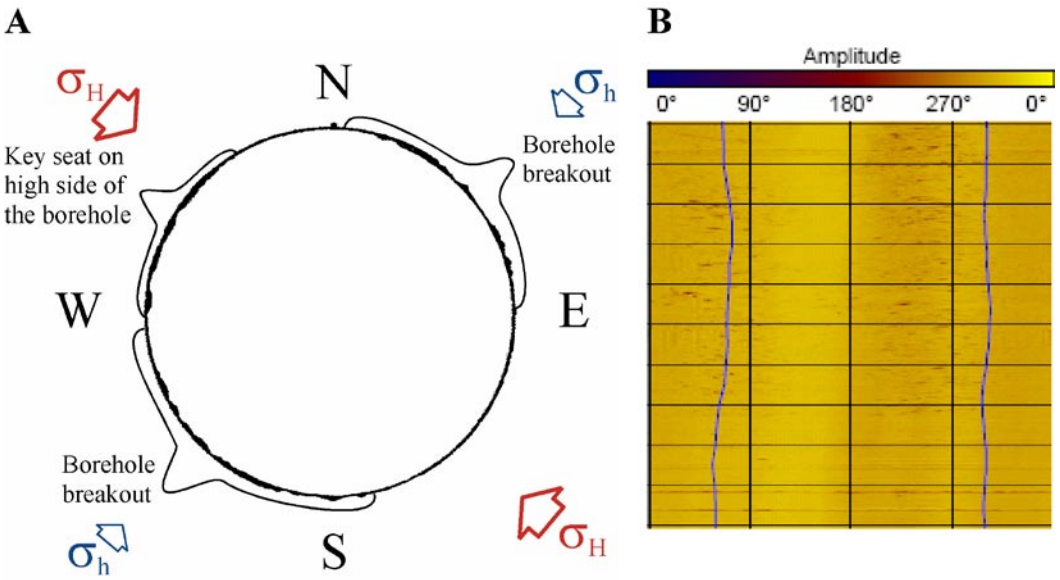

Figure 4-3. *Examples of views that are used for analysis of BHTV data, from borehole KFM01A. A) Borehole cross section of CALIPER 3D data, from near 946 mbl. An interpretation of the image is also included. B) Unwrapped amplitude image, from 945.0 to 947.0 mbl. Modified from /Nielsen and Ringgaard 2003/.*

5 Results of initial breakout identification

5.1 General

The two boreholes KFM01A and KFM01B were drilled within 20 m from each other to 1,001.45 and 500.52 m borehole length (mbl), respectively, at Drill Site 1. Borehole KFM01A is of "telescope" type with the upper 100 m percussion drilled with larger diameter (250 mm) and cased. The sections below 100 m of borehole KFM01A and the entire borehole KFM01B were diamond-drilled with 77 and 76 mm diameter bit size, respectively. Boreholes KFM01A and KFM01B are dominated by a medium-grained metagranodiorite-granite, although finer grained metagranitoids, pegmatitic granites, amphibolites and minor bands, dykes or veins of leucogranitic material also were recovered /Petersson and Wängnerud 2003, Berglund et al. 2004/. With a few exceptions, the rocks exhibit a moderate to steep ductile foliation, striking roughly between NW-SE and NNE-SSE in borehole KFM01A /Petersson and Wängnerud 2003/, and NW-SE in borehole KFM01B /Berglund et al. 2004/.

Figure 5-1 shows the results from BHTV logging in boreholes KFM01A and KFM01B. At the ground surface, borehole KFM01A has a borehole azimuth of 318°N and a deviation versus horizontal of 85° (hence 5° versus vertical). Near the base of the borehole, the corresponding values are 307°N and 75°, respectively (~300°N/~74° according to /Nielsen and Ringgaard 2003/). Borehole KFM01B has an azimuth at the surface of 268°N and a deviation versus horizontal of 79°. At 500 mbl, the borehole azimuth is 271°N and the deviation is 71° (~276°N/~72° according to /Nielsen and Ringgaard 2004/). No centralizers were used during BHTV logging in borehole KFM01A, whereas such equipment was used in borehole KFM01B /Nielsen and Ringgaard 2003, 2004/.

No clear or continuous borehole breakouts are observed at the scale presented in Figure 5-1, but closer inspection of the data at a more detailed scale reveals that both stress- and drilling induced features are influencing the borehole geometry. We will first present results regarding borehole elongations caused by the drilling- and logging processes that cannot be coupled to the stress field (drilling induced features such as key seats, washouts and grooves). This is followed by a presentation of stress-induced features (breakouts and DIFs) that have been observed in the data.

Six clearly visible fallouts in borehole KFM01B (both breakouts and washouts) were chosen from BHTV amplitude data for a more in depth study of the geology. Because the geology cannot be determined using amplitude data, the selection may be regarded as random. The results entail that four fallouts are related to heavily metamorphorized amphibolite (rock type code 102017). The amphibolite is medium to coarse grained and often shows signs of foliation in the form of schistocity due to parallel orientation of amphibole or biotite crystals /Loberg 1999/. Thus, these fallouts appear to be located in zones with reduced strength. The remaining two fallouts are located in what appears to be homogeneous granite/granodiorite (rock type code 101057) with few fractures. In one case, laumontite fracture fillings are present.

We emphasize that, because we only have access to the WellCAD Reader, the depth estimates of drilling- and stress induced elongations are only approximate and likely overestimations (only the maximum anomaly can be determined).

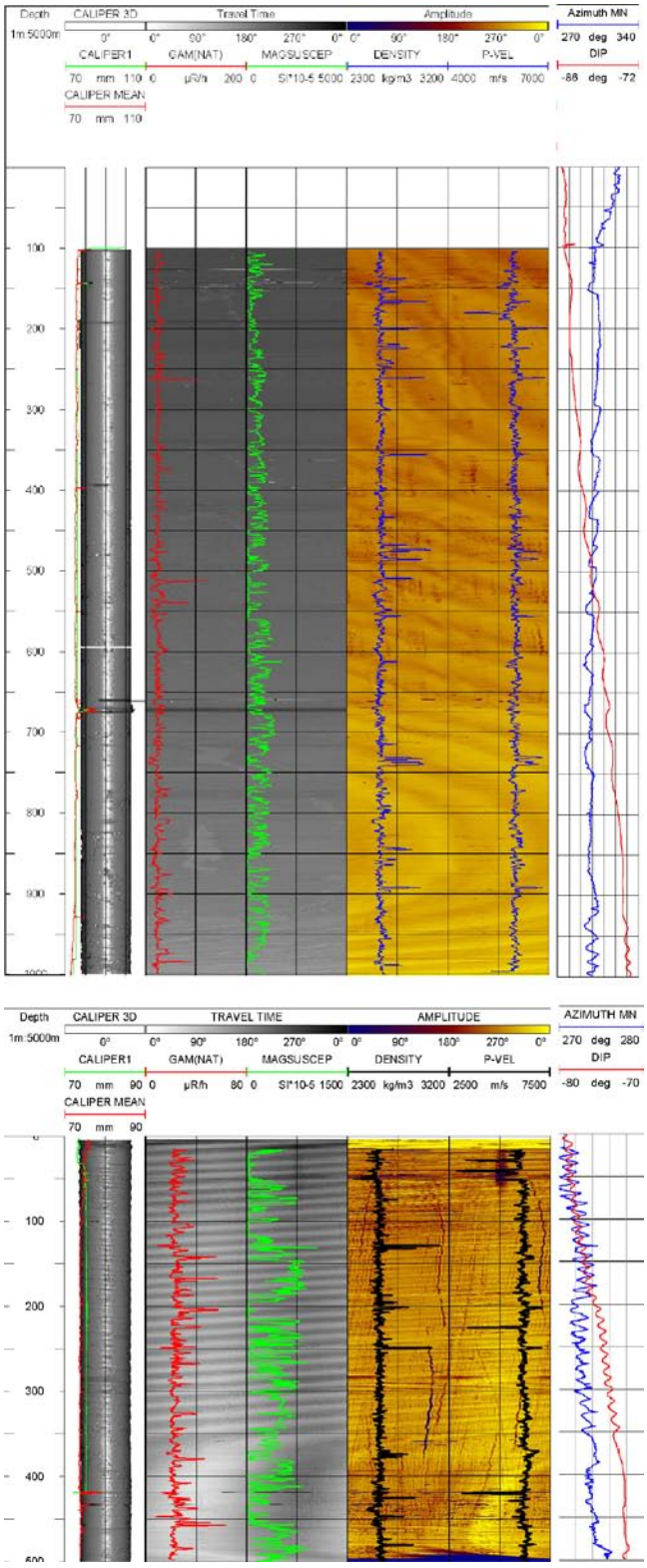

Figure 5-1. *Results from BHTV logging in boreholes KFM01A (top) and KFM01B (bottom). Data from /Nielsen and Ringgaard 2003, 2004/.*

5.2 Drilling-induced elongations

We observe four groups of drilling-induced elongations: (1) key seats, (2) washouts, (3) sub-horizontally inclined grooves, and (4) sub-vertically inclined grooves. Most of these features were found in borehole KFM01B.

A pronounced key seat (about 15–30° wide and 1–2 mm deep) was identified between 15 and 60 mbl in borehole KFM01B (Figure 5-2) on the high side of the borehole wall, parallel to the borehole azimuth. We also observed three narrow sub-vertical grooves from about 50 to 120 mbl (Figure 5-2). This was followed by 1–2 mm deep narrow grooves with a spacing of about 2.5 m on the lower side of the borehole. Most likely, these features are a result of a rapid change of borehole direction (i.e. a kink at about 50–60 mbl) or a large feeding force during drilling, giving a bend on the drill pipe. Because no rapid change in borehole direction was found during deviation measurements /Berglund et al. 2004, Nielsen and Ringgaard 2004/, the phenomenon is most likely related to a large feeding force during drilling.

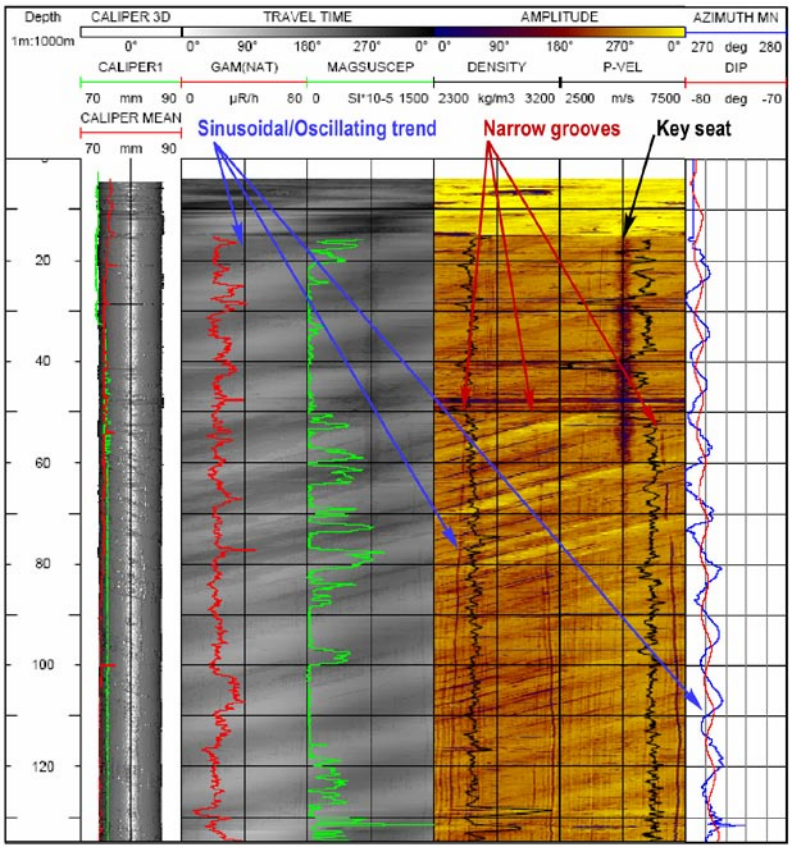

Figure 5-2. *Some drilling-induced features in borehole KFM01B. A pronounced key seat (black arrow) is observed from about 15 to 60 mbl, at 270° azimuth, which is parallel to AZIMUTH MN, the direction of the borehole. Three distinct narrow grooves are also observed from about 50 to 120 mbl (red arrows), together with a number of less distinct sub-axial grooves. These are interpreted as drilling-induced features or a result of wear of different borehole equipments during hoisting and lowering operations in the borehole. Throughout the interval, the BHTV images display sinusoidal and oscillating downhole trends (blue arrow). These may be drilling induced or, alternatively, an effect of decentralized tool during logging. Modified from /Nielsen and Ringgaard 2004/.*

A washout appears as an increase in all dimensions of the borehole and is commonly associated with fallouts in pre-existing fractures or fracture zones. We found one large washout near 419 mbl in borehole KFM01B (Figure 5-3), where pre-existing fractures have caused significant fallout of material. The washout is related to a heavily metamorphorized amphibolite (rock type code 102017). The rock is fractured with both open and sealed fractures and with a breccia immediately above the amphibolite. The same washout, but displayed as BIPS image and BHTV amplitude, is given in Figure 5-5. The example indicates a slight depth difference between the two systems (0.6 m; see Chapters 6.3 and 7).

We observed sinusoidal patterns in downhole variation of borehole azimuth (AZIMUTH MN) and borehole inclination data from horizontal (DIP) over several sections in both boreholes. These oscillations are clearly picked up by the travel time and amplitude images as well. The most significant trend is observed from the surface to 350 mbl in borehole KFM01B, for which the AZIMUTH MN varies by about 10°N and the DIP varies by 1° over ~15 m long periods (Figure 5-1). Additionally, some BIPS images in the investigated boreholes have sporadically occurring spiral-type dark coatings on the borehole wall with a pitch ratio of 12–13 cm (Figure 5-6). /Petersson and Wängnerud 2003/ suggested that these grooves were drilling-induced, although the mechanism is not fully understood. Alternate and/or complementary interpretations of these patterns are that they could be measurement related and caused by a decentralized BHTV tool. Possibly, but perhaps less likely, the pattern reflects stick-slip behaviour of the tool during logging. This question can be solved when analyzing the raw, unprocessed data from the BHTV logging, see Chapter 7.

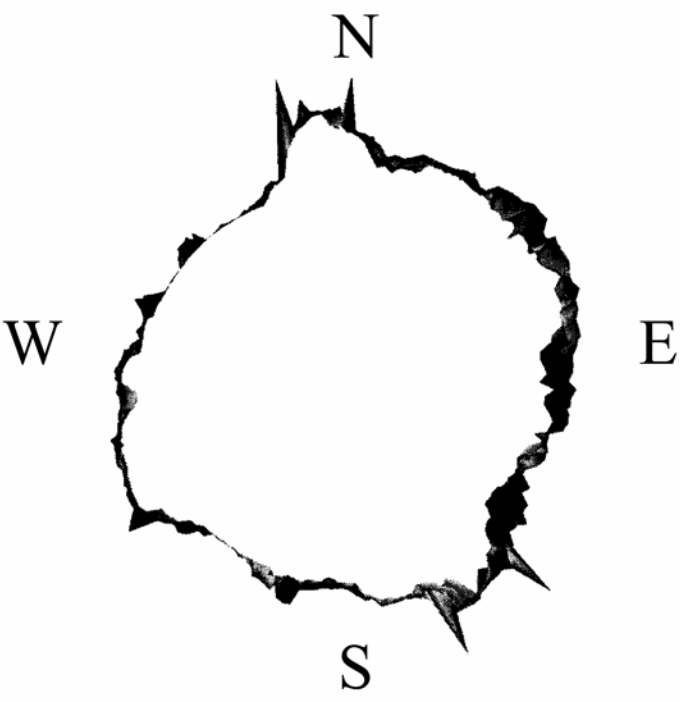

Figure 5-3. *Washout in borehole KFM01B at 419 mbl (the cross sectional view of the borehole has a section thickness of 5 mm (data from /Nielsen and Ringgaard 2004/).*

Figure 5-4. *Drill core at the depth of the washout in borehole KFM01B at 419 mbl (core box no 78).*

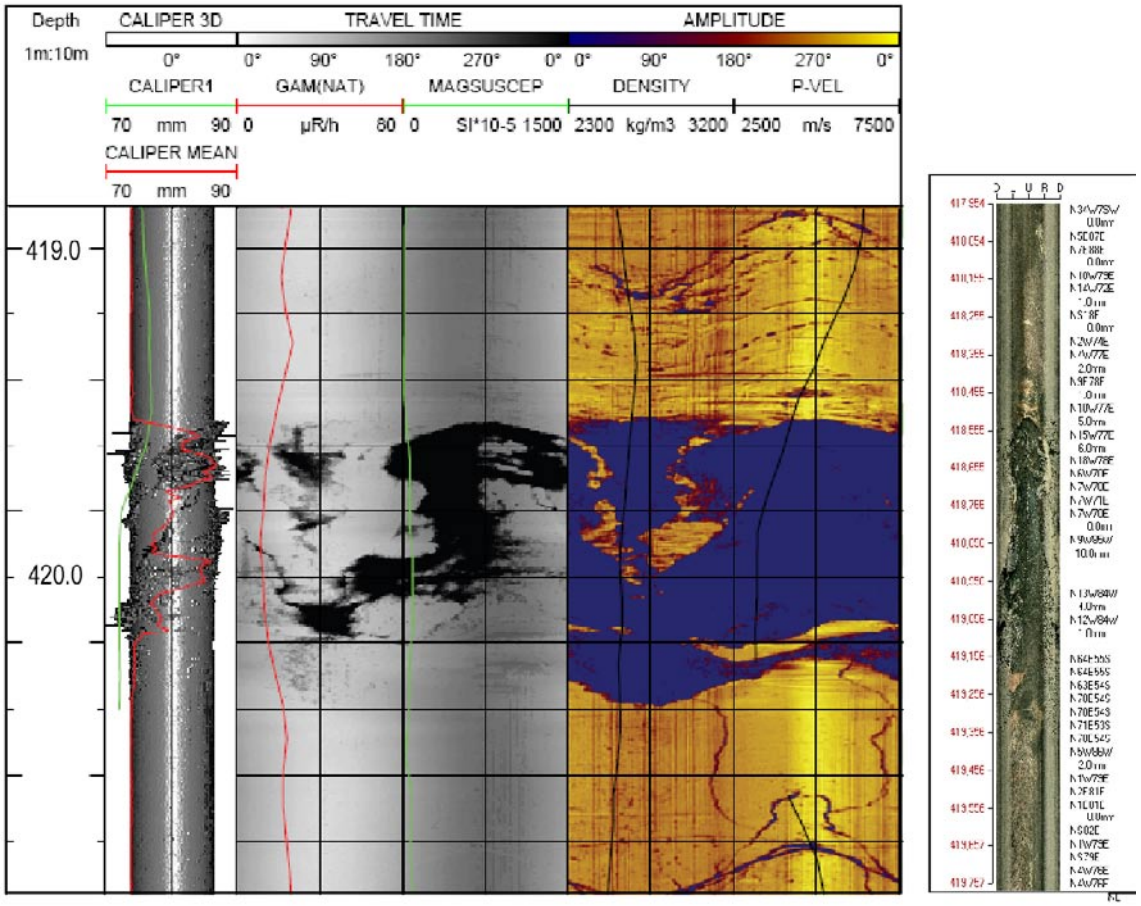

Figure 5-5. *Washout near 419 mbl in borehole KFM01B. Results from the BHTV and BIPS logs at the same scale. This representation clearly reveals the offset in depth data between the two data sets. Data from /Nielsen and Ringgaard 2004/ and /Gustafsson and Gustafsson 2004/.*

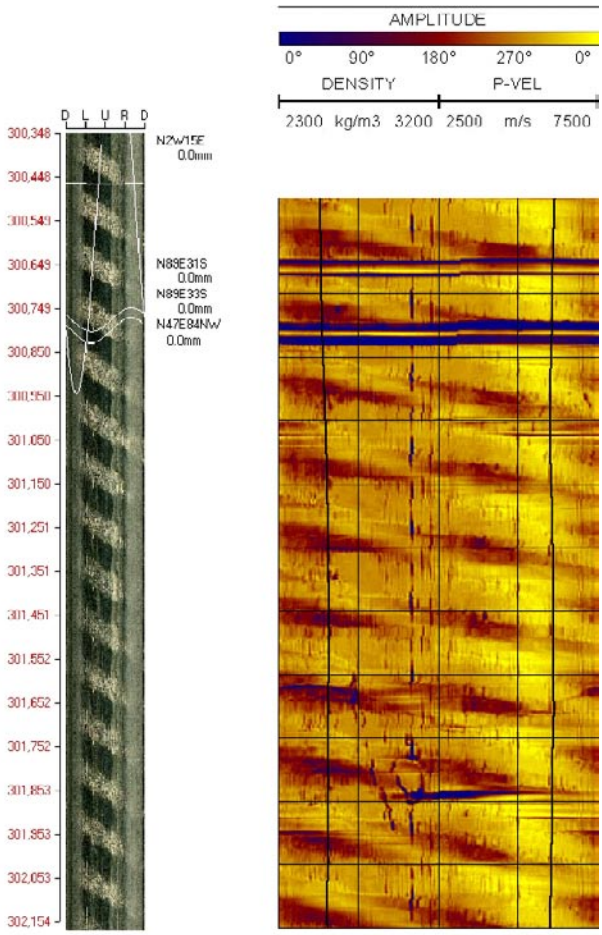

Figure 5-6. *The borehole wall contains a spiral-shaped pattern, near 300 mbl in borehole KFM01B. Results from the BIPS log with structural interpretations. Red text shows adjusted depth (mbl; left). Data from /Nielsen and Ringgaard 2004/ and /Gustafsson and Gustafsson 2004/.*

5.3 Stress-induced elongations

As noted above, no large scale borehole breakouts were observed in Figure 5-1. However, numerous borehole breakouts were identified in both boreholes when the data were inspected at a more detailed scale. The boreholes fail in the direction of the minimum horizontal stress, σ_h; hence, the orientation of the maximum horizontal stress, σ_H, is 90° off.

5.3.1 KFM01A

Borehole breakouts have been detected in several sections of the borehole, from 112 mbl to 1,001 mbl (Table A1-1). In total, the results from this initial analysis suggest that borehole breakouts had been formed in about 277 m of the total 1,001 m borehole length at the time of logging, i.e. about 28% of the logged borehole length contains borehole breakouts. The breakouts show a consistent orientation of σ_H, about NW-SE, which indicates that the stress field is continuous with small influence of pre-existing structures on the prevailing stress field in the rock mass.

The majority of breakouts are wide (e.g. about 90° at 946 mbl in KFM01A, Figure 4-3A), but their failure depths are shallow, which explains that the breakouts generally have not been identified using the BIP system. In general, the breakouts appear as two diametrically opposite zones in which grain-sized fallouts have appeared.

At a few locations, deeper and more rugged breakouts were identified (Figure 5-7). These were easily observed in both BHTV and BIPS. Often, these sections appeared to be partly washed out as well (cf Figure 3-5), but nevertheless, they are thought to provide some information on stress orientation.

The depths of borehole breakouts are best visualized by stacking CALIPER 3D data over a borehole cross section plot of a 5-mm thick slice (Figure 5-7). The widths of breakouts, on the other hand, are best viewed on unwrapped amplitude logs (Figure 5-8 and Figure 5-9). This is especially characteristic for breakouts with small failure depth. Individual spikes (e.g. Figure 5-7) probably reflect faulty detection in the BHTV data, due to the fact that the surface of the borehole wall is highly over-sampled with respect to caliper variation as the sampling interval is defined by the desired high resolution of the amplitude image /Deltombe and Schepers 2000/.

The vast majority of borehole breakouts, especially the ones with shallow failure depth, could only be identified in the BHTV log. The BIPS images could only identify major breakout zones in which clear fractures had been formed. One exception of the applicability of the BIPS system is for borehole sections that occur in the amphibolite, which has a dark colour. In these sections, the BIPS images display grain-size reflections on diametrical sides of the borehole wall (Figure 5-10).

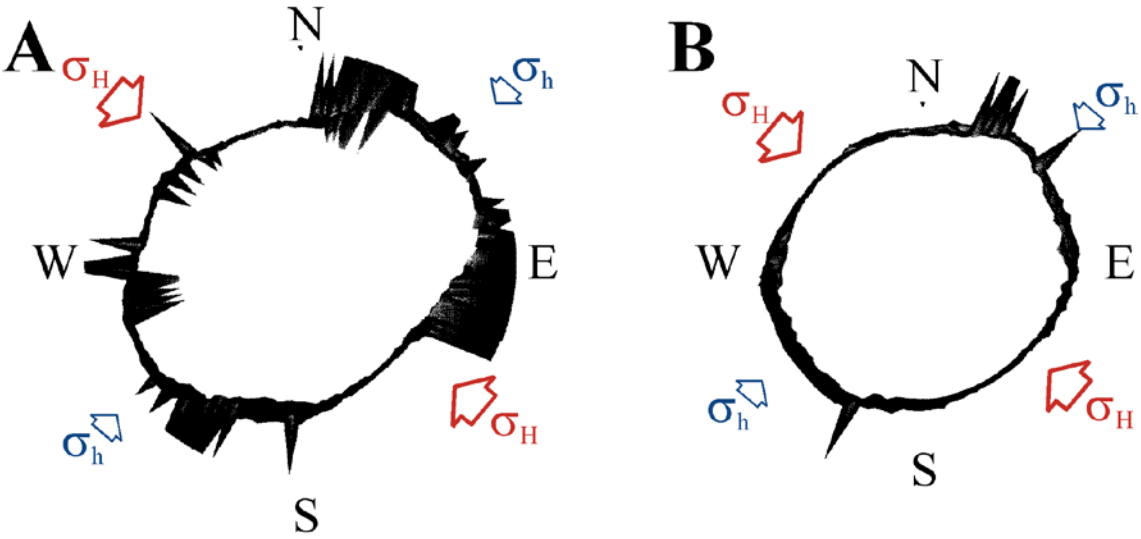

Figure 5-7. *Examples of breakouts in borehole KFM01A at 929 (A; breakout/washout) and 982 mbl (B) where the orientation of the horizontal stresses may still be determined (section length 5 mm). Data from /Nielsen and Ringgaard 2004/.*

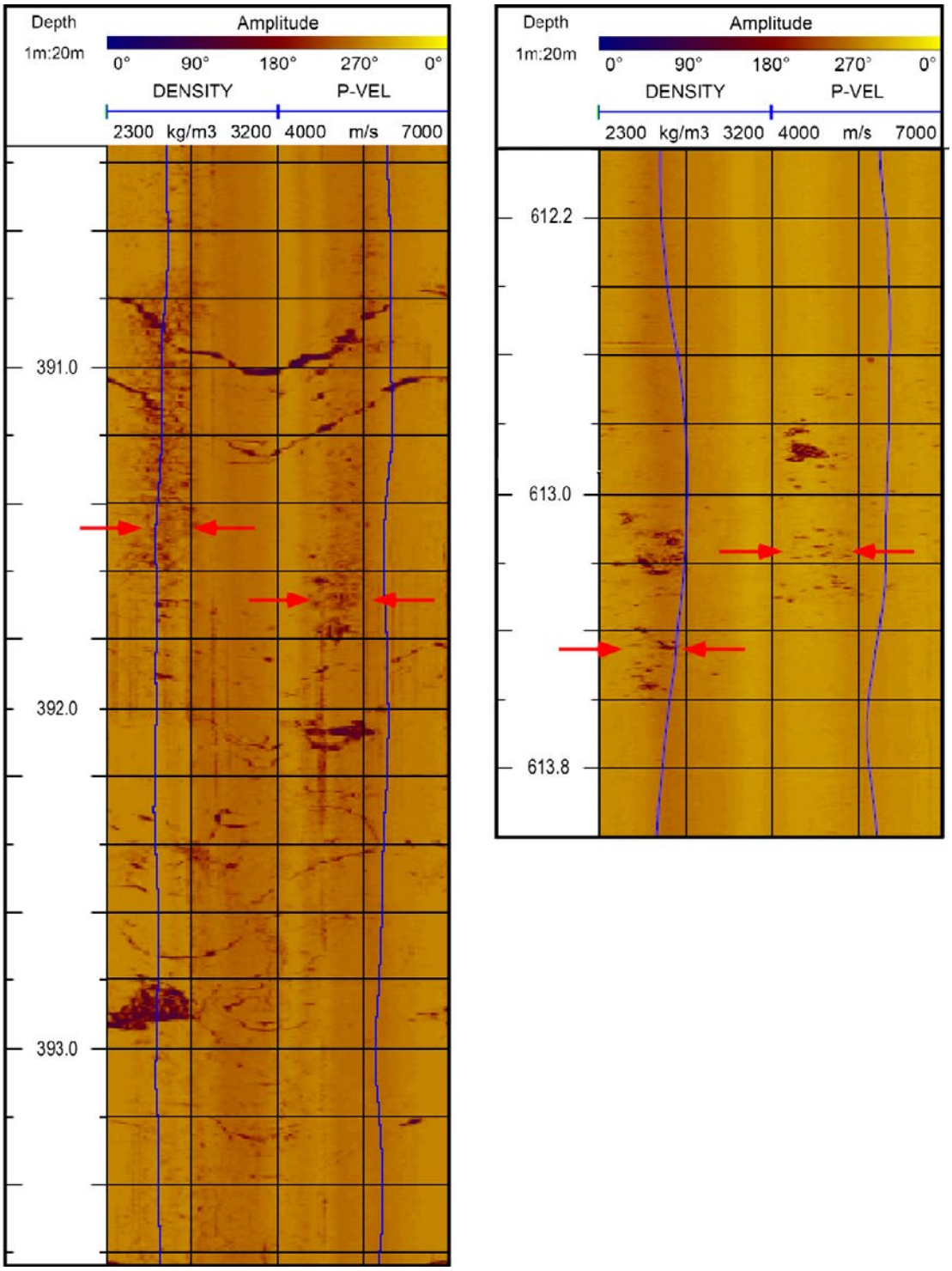

Figure 5-8. *Examples of BHTV amplitude log images of borehole breakouts in borehole KFM01A. Left, from 390.4 to 393.6 mbl; Right, from 612.0 to 614.0 mbl. Red arrows indicate approximate breakout widths (modified from /Nielsen and Ringgaard 2004/).*

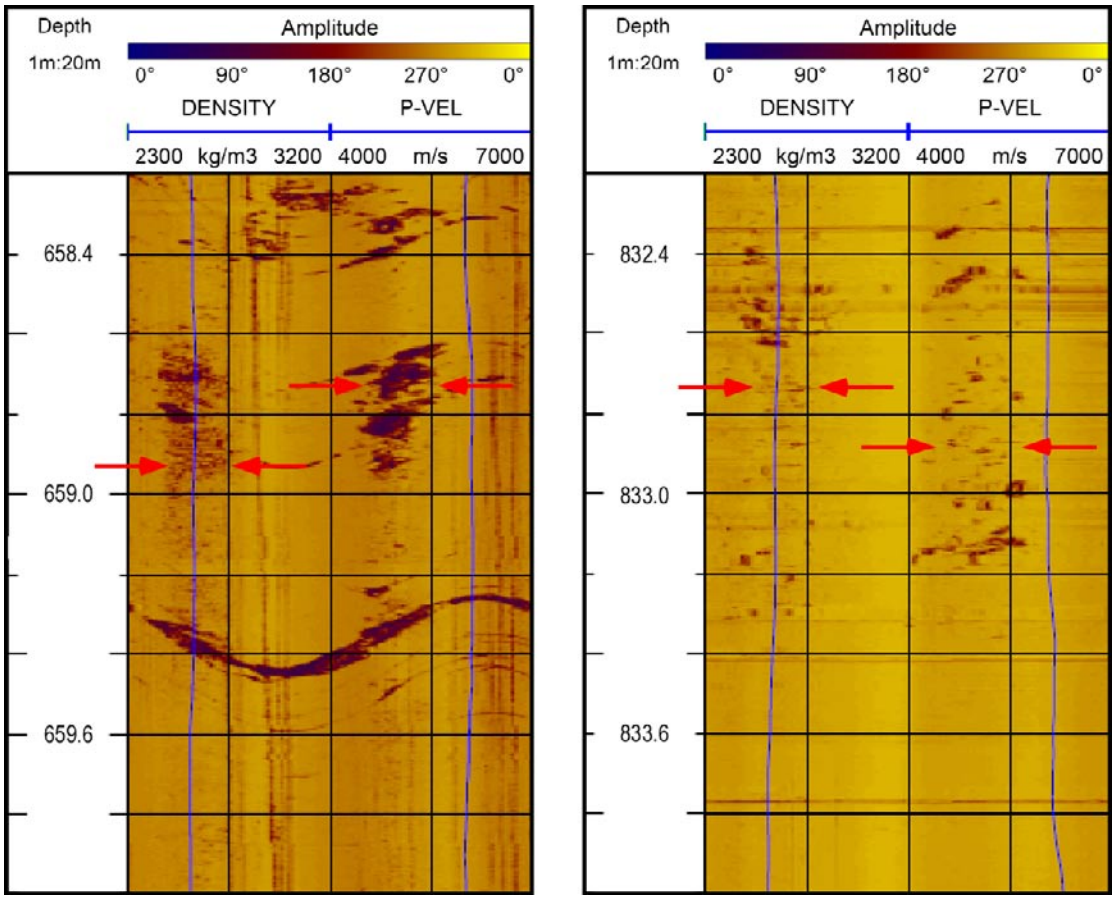

Figure 5-9. *Examples of BHTV amplitude log images of borehole breakouts in borehole KFM01A. Left, from 658.2 to 660.0 mbl; Right, from 832.2 to 834.0 mbl. Red arrows indicate the breakout width (modified from /Nielsen and Ringgaard 2004/).*

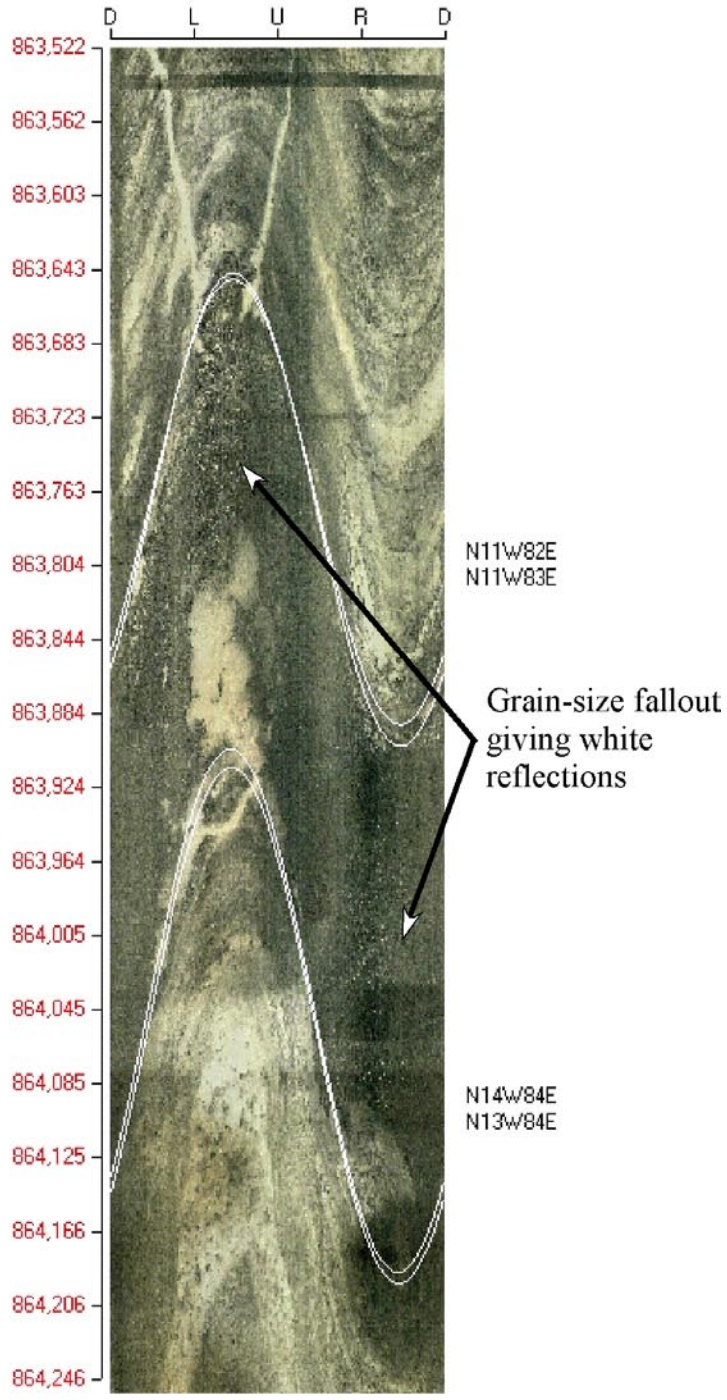

Figure 5-10. *Grain-size fallout in amphibolite rock giving white reflections on BIPS image (data from 864 mbl in borehole KFM01A; /Petersson and Wängnerud 2003/).*

5.3.2 KFM01B

The results of the analyses propose that borehole breakouts exist in several sections of the borehole, from 113 mbl to 499 mbl (Table A2-1). In total, this initial study suggests that borehole breakouts occur over almost 40% of the borehole length, or about 195 m of the total 500 mbl. As in borehole KFM01A, most of these were identified using acoustic BHTV log.

The breakouts show a consistent orientation of σ_H of about NW-SE, have a large width but a limited depth, with exception for the major breakout from 432.0–435.2 mbl (Figure 5-11 to Figure 5-15). The failure depths are visualized by a cross section plot, whereas the widths, especially the breakout with small failure depth, are most easily viewed on amplitude logs.

The major breakout is located in what appears to be homogeneous granite-granodiorite (rock type code 101057). In the lower part of the section also pegmatite appears (rock type code 101061) as well as fractures filled with laumontite (Figure 5-16 and Figure 5-17).

An additional stress-induced elongation, drilling-induced fractures (DIFs), may have been formed in borehole KFM01B. Two sub-parallel, diametrically opposed grooves were observed from 50 to 225 mbl, and from 225 to 380 mbl (Figure 5-18). Their appearance (narrow, wiggling, and diametrically opposed fractures) resembles the appearance of drilling induced fractures (DIFs; e.g. /Brudy and Zoback 1993, Peska and Zoback 1995, Zoback et al. 2003/), and they are oriented about 90° from identified borehole breakouts in this borehole. If these grooves indeed are DIFs, they indicate a small shift in the orientation of σ_H, from a NNW-SSE orientation in the shallower interval to a NW-SE orientation in the deeper interval. These orientations agree well with those obtained from borehole breakouts, see further Chapter 6.2.

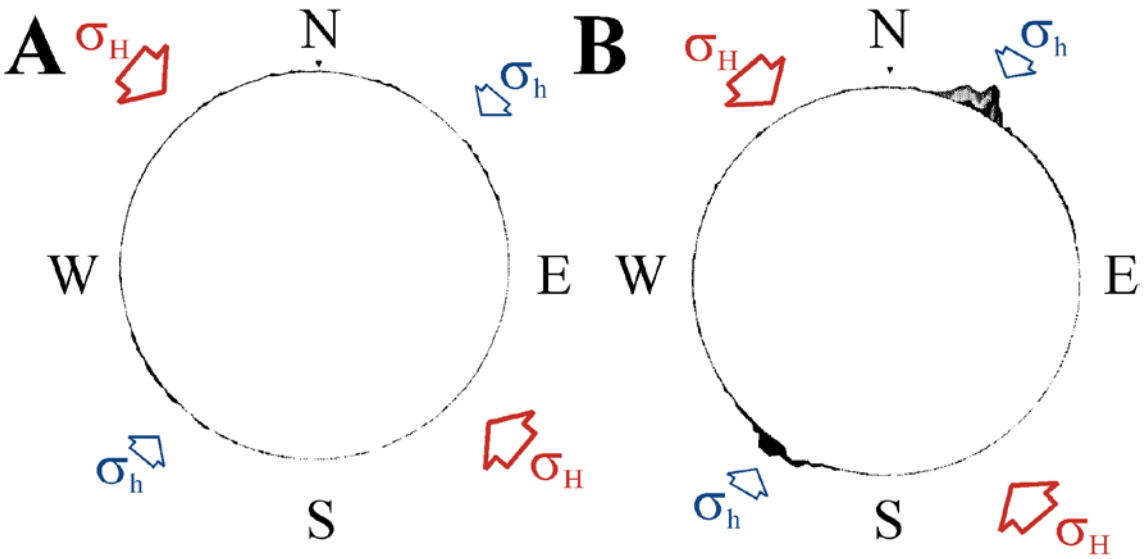

Figure 5-11. *Examples of shallow-located borehole breakouts in borehole KFM01B at 133 (A; clearly observed on amplitude log) and 218 mbl (B; section length 5 mm). Data from /Nielsen and Ringgaard 2004/.*

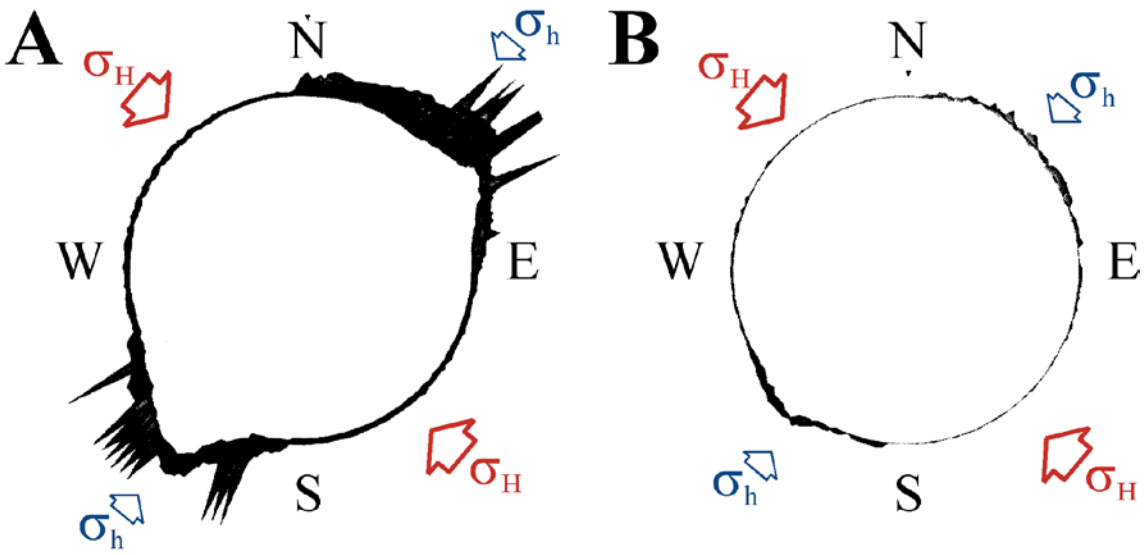

Figure 5-12. *Examples of deeper-located and pronounced borehole breakouts in borehole KFM01B at 433 (A) and 464 mbl (B; section length 5 mm). Data from /Nielsen and Ringgaard 2004/.*

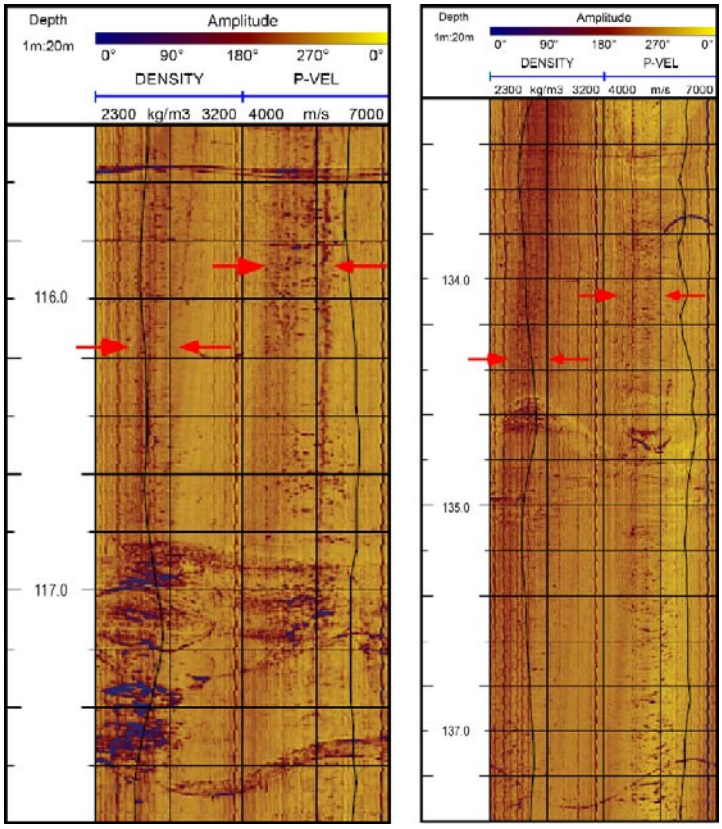

Figure 5-13. *Examples of BHTV amplitude log images of borehole breakouts in borehole KFM01B. Left, from 115.4 to 117.8 mbl; Right, from 133.2 to 137.4 mbl. Red arrows indicate the breakout width (modified from /Nielsen and Ringgaard 2004/).*

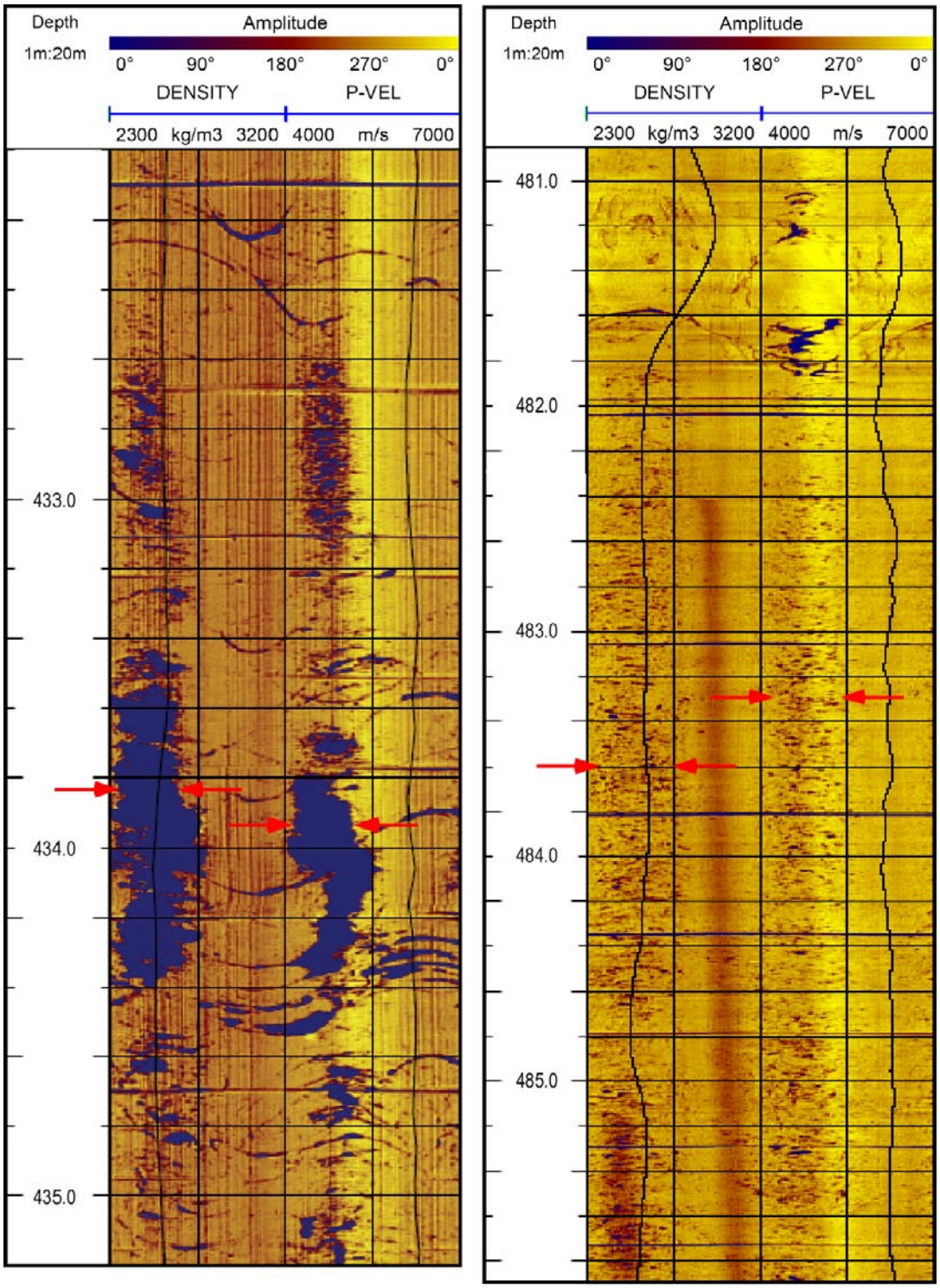

Figure 5-14. *Examples of BHTV amplitude log images of borehole breakouts in borehole KFM01B. Left, from 432.0 to 435.2 mbl; Right, from 480.8 to 486.0 mbl. Red arrows indicate the breakout width (modified from /Nielsen and Ringgaard 2004/).*

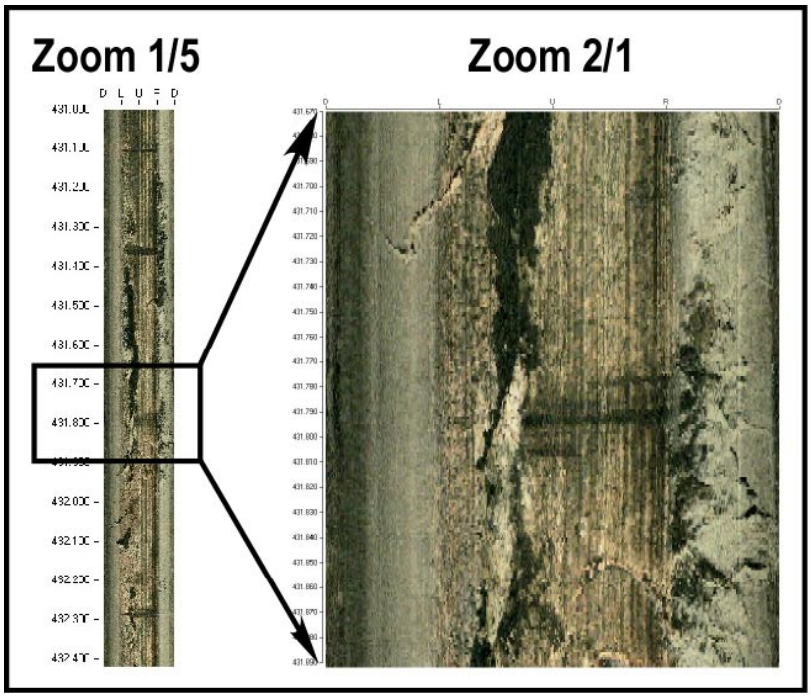

Figure 5-15. *Borehole breakout detected by the BIPS camera near 432 mbl in borehole KFM01B. The fractures are clearly seen in at the detailed scale (Zoom 2/1.) Modified from* /Berglund et al. 2004/.

Figure 5-16. *Drill core at the level of the major breakout in KFM01B at 432.0–435.2 mbl (lower core box, no 80).*

Figure 5-17. *Drill core at the level of the major breakout in KFM01B at 432.0–435.2 mbl (upper core box, no 81).*

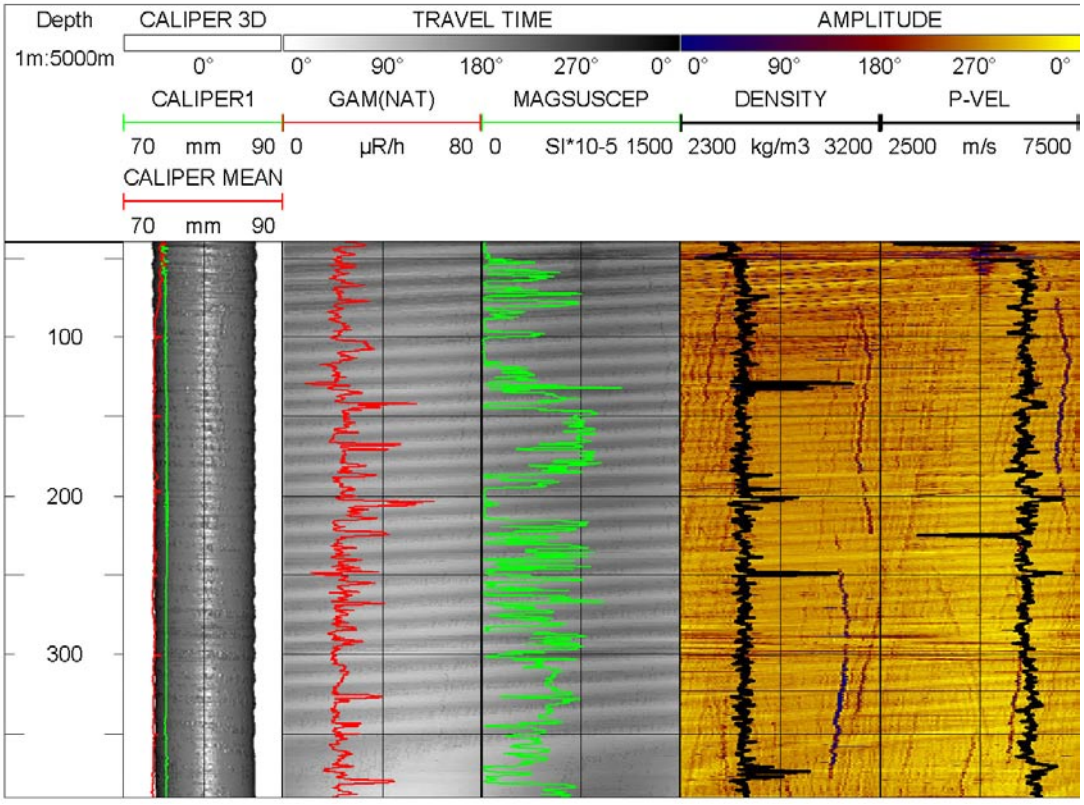

Figure 5-18. *Potential occurrence of drilling-induced fractures (DIFs) from 50 to 380 mbl in borehole KFM01B. If the diametrically opposed grooves indeed are DIFs, they suggest a NNW-SSE to NW-SE orientation of the maximum horizontal stress (data from /Nielsen and Ringgaard 2004/).*

6 Discussion of results and examples of detailed characterization of breakout

In this chapter, the results and implications of the stress-induced elongations are discussed. This is continued by a description of how borehole breakouts are characterized with a brief analysis of stress magnitudes of selected borehole breakouts in borehole KFM01B.

6.1 Observed breakout types in boreholes KFM01A and KFM01B

The identified breakouts in boreholes KFM01A and KFM01B appear from about 115 mbl. Two main types of borehole breakouts were found in the investigated boreholes: (1) Well-developed, deep borehole breakouts that are easy to detect in both BHTV and BIPS logs; and (2) Borehole breakouts with small failure depths that are undetectable in BIPS data but clearly revealed in the BHTV amplitude log and to some extent in cross section plots of the borehole geometry. Both breakout types have a width of up to 90° but the former have a V-shaped failure surface whereas the latter have a broad flat-bottomed surface. The borehole breakout widths of about 90° are in accordance with other reported breakouts, e.g. /Barton et al. 1988, Zoback et al. 1985/, and /Berard and Cornet 2002/, cf. Figure 6-1.

It is neither unexpected nor unusual that the type and shape of borehole breakouts vary within an individual borehole, because borehole breakout shape and type depend on rock strength, depth, and state of stress /Plumb 1989/. We note that the magnitude of the tangential stresses in both boreholes are approximately of the same order as those of crack initiation strength of the dominant lithology (metagranodiorite-granite; see Chapter 6.1.2), which may explain that the majority of the borehole breakouts have a limited failure depth. The minority of borehole breakouts are well developed, and our initial analysis propose that they tend to occur in darker rocks (amphibolites), i.e. they are located in zones of reduced compressive strength (and possibly also in high-stress zones). In addition to downhole variation of the parameters rock strength, depth, and state of stress, another explanation would be that the breakouts with limited failure depths represent initial stages of breakout formation. Previous studies have shown that only the breakout depth increases with time, not the width /e.g. Zoback et al. 1985/. These authors concluded that a complex process is responsible for breakout growth, e.g. in-elastic deformation and time-dependent deformation (creep).

The time period between drilling and logging with BHTV was longer in borehole KFM01A than in borehole KFM01B (about 7.5 and 1.5 months, respectively). Furthermore, at the Forsmark site, it is conceivable that the vertical stress is the least principal stress down to considerable depths. Thus, borehole KFM01A has slightly larger tangential stresses compared with borehole KFM01B. With these time and stress effects, one would expect that breakouts are more developed in borehole KFM01A compared with KFM01B. However, surprisingly, the opposite situation prevails, which implies that the time effect for breakout development may be negligible. Possibly, this may be explained by the overcoring measurement campaign in borehole KFM01B, which involves numerous lowering and hoisting operations. During these activities, it is probable that loose material has been eroded away giving more pronounced breakouts.

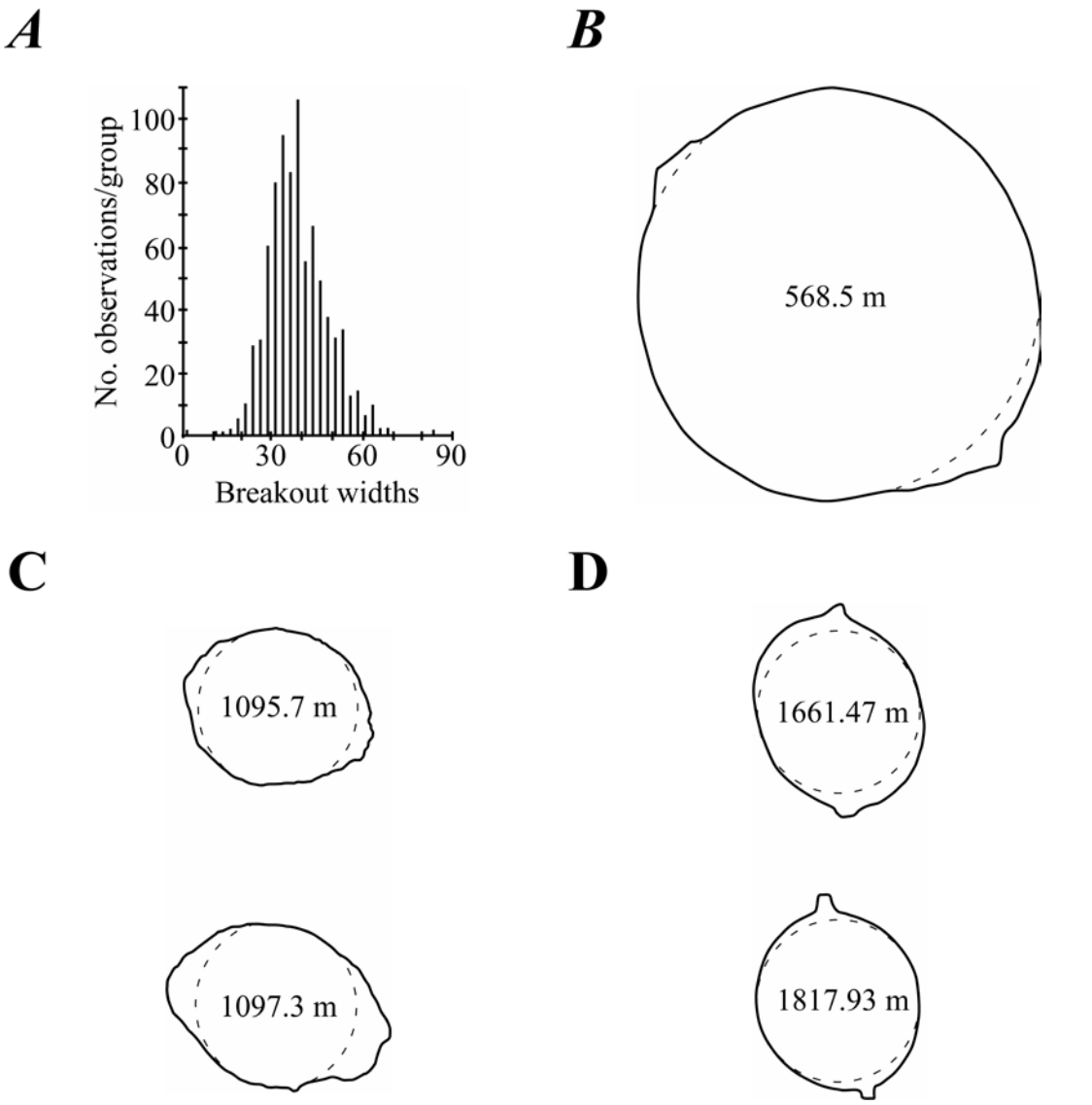

Figure 6-1. *Histograms of breakout widths (half width) at the Fenton well, New Mexico /A; Barton et al. 1988/ and examples of breakouts at Montecillo, South Carolina /B; Zoback et al. 1985/, the Nevada test site /C; Zoback et al. 1985/, and Soultz-sous-Forêts /D; Berard and Cornet 2002/.*

Broad breakouts with flat-bottomed failure surfaces, are frequently reported in different geological settings. E.g. /Zoback et al. 1985/ presented results from breakouts in Paleozoic sandstone, granite, and tuff. These breakouts cannot be explained by the outlined theory in Chapter 3.2. /Zoback et al. 1985/ presented a simple theory based on the Mohr-Coulomb criterion that explains the occurrence of broad and flat-bottomed breakouts, which is summarized below.

A more detailed characterization of borehole breakouts was undertaken for the three deeper breakouts observed in borehole KFM01B at 218, 433, and 464 mbl (Figure 5-11 and Figure 5-12). These breakouts were used for estimation of horizontal stress magnitudes using the empirical method of /Martin et al. 1999/. The key data for the breakouts are visualized in Figure 6-2 and involve the angle α, i.e. the orientation of the breakout with respect to North, the borehole radius R, the width of the breakout, φ_b, and the failure depth of the breakout, r_b.

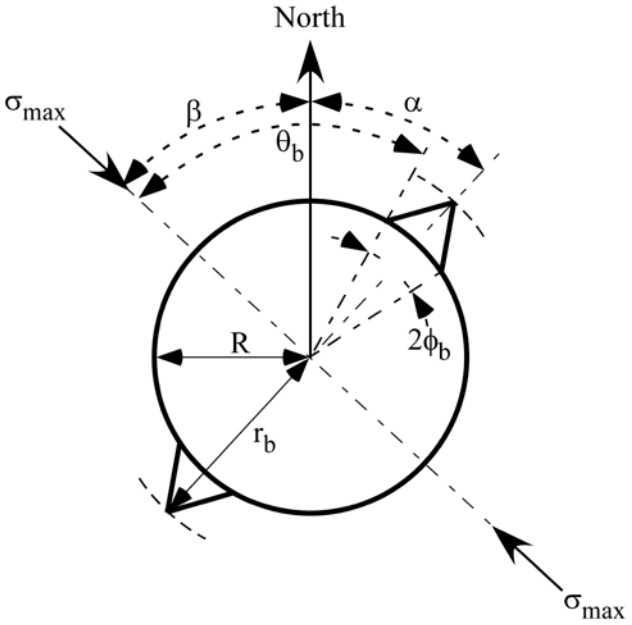

Figure 6-2. *Key data for breakout analysis involve the orientation of the breakout, α, and maximum horizontal stress, β, respectively, with respect to North, the borehole radius R, the width of the breakout, φ_b, and the failure depth of the breakout calculated from the centre of the borehole, r_b.*

6.1.1 Broad, flat-bottomed borehole breakouts

Breakout widths

The theoretical relationship for applied far-field stresses described by /Kirsch 1898/, and subsequently by others /e.g. Jaeger and Cook 1969/, are given in Equations (1) to (3) (see Chapter 3.2). These equations show that the magnitude of shear and effective normal stress varies as a function of r and θ. The region of compressive shear failure can be predicted by the extended Griffith criterion /McClintock and Walsh 1962/, which considers the extension of closed fractures, which have a finite frictional strength in a biaxial stress field. The analysis is equivalent with the Coulomb criterion in which the failure envelope has a slope equal to the coefficient of sliding, μ (μ =tan φ, where φ is the internal friction angle), and an intercept τ_o equal to the cohesive strength of the rock, C. According to the Mohr-Coulomb criterion, the shear stress, τ, and the effective normal stress, σ, on the failure surfaces are related as:

$$|\tau| = C + \mu \cdot \sigma \tag{9}$$

or rearranged

$$C = \left(1+\mu^2\right)^{1/2} \cdot \left(\left(\frac{\sigma_\theta - \sigma_r}{2} \right)^2 + \tau_{r\theta}^2 \right)^{1/2} - \mu \cdot \left(\frac{\sigma_\theta + \sigma_r}{2} \right) \tag{10}$$

Equations (1) to (3) may be substituted in Equation (10), thereby expressing C in terms of r, θ, and the horizontal principal stresses (Figure 6-2). Conversely, for given values of the horizontal principal stresses, C, and μ, the extent of the breakout zone where shear failure occurs can be determined. When neglecting the excessive fluid pressure in the borehole (i.e. $\Delta P = 0$), /Zoback et al. 1985/ showed that: (1) for given values of C and μ, an increasing σ_H/σ_h-ratio makes the breakout much larger and with steeper edges; (2) for given values of stress ratio and C, an increasing μ makes the breakout much smaller; and (3) for given values of stress ratio and μ, a decreasing C makes the breakout deeper and wider.

The theory can be extended to the general problem of initial size of breakouts in terms of rock cohesive strength, coefficient of friction, and excessive fluid pressure. Equations (1) to (3) and (10), assuming $\Delta P = 0$, can be used to describe the cohesive strength at the points of maximum (R,θ_b) and minimum $(r_b,\theta_b, \pi/2)$ tangential stress:

$$C(R,\theta_{b/2}) = 0.5 \cdot (a \cdot \sigma_H + b \cdot \sigma_h) \tag{11}$$

$$C(r_b,\pi/2) = 0.5 \cdot (c \cdot \sigma_H + d \cdot \sigma_h) \tag{12}$$

where

$$a = \left[\left(1+\mu^2\right)^{1/2} - \mu\right] \cdot [1 - 2 \cdot \cos \cdot 2\theta_b] \tag{13}$$

$$b = \left[\left(1+\mu^2\right)^{1/2} - \mu\right] \cdot [1 + 2 \cdot \cos \cdot 2\theta_b] \tag{14}$$

$$c = -\mu + \left(1+\mu^2\right)^{1/2} - \frac{R^2}{r_b^2} \cdot \left[\left(1+\mu^2\right)^{1/2} + 2 \cdot \mu\right] + 3 \cdot \frac{R^4}{r_b^4}\left(1+\mu^2\right)^{1/2} \tag{15}$$

$$d = -\mu - \left(1+\mu^2\right)^{1/2} + \frac{3 \cdot R^2}{r_b^2}\left[\left(1+\mu^2\right)^{1/2} + 2 \cdot \mu\right] + 3 \cdot \frac{R^4}{r_b^4}\left(1+\mu^2\right)^{1/2} \tag{16}$$

Consider a breakout which follows the trajectory for a given value of the cohesive strength such that $C(R,\theta_b) = C(r_b, \pi/2) = C$. Solving Equations (11) and (12) for the stresses will then yield:

$$\sigma_H = 2 \cdot C \cdot \frac{d-b}{a \cdot d - b \cdot c} \tag{17}$$

$$\sigma_h = 2 \cdot C \cdot \frac{a-c}{a \cdot d - b \cdot c} \tag{18}$$

$$\frac{\sigma_H}{\sigma_h} = \frac{d-b}{a-c} \tag{19}$$

Figure 6-3 graphically shows the σ_H/σ_h-ratio (independent of *C)* as a function of R/r_b and φ_b (where $\varphi_b = \pi/2 - \theta_b$, see Figure 6-2). In the example, μ was set to 0.6, which corresponds to an internal friction angle of 31° (Paleozoic sandstone in Auburn, New York; /Zoback et al. 1985/) and the σ_H/σ_h-ratio was limited to 3. The figure indicates that when σ_H and σ_h are almost equal, little spalling is anticipated. Moreover, as the breakouts get deeper and wider with increasing σ_H/σ_h-ratio, the well bore radius increases by only about 15% when φ_b is as large as 50°. Hence, this theory can explain broad flat-bottomed breakouts but not deeper breakouts.

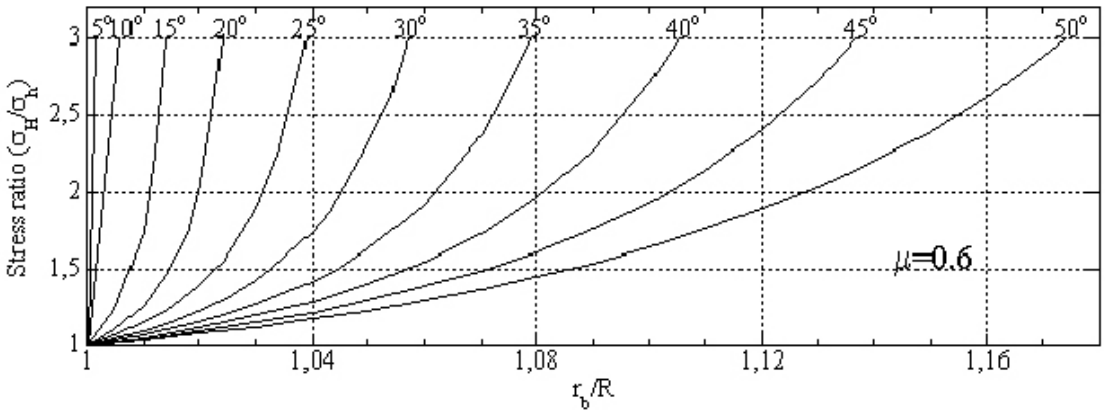

Figure 6-3. *Relationship between the ratio of the horizontal principal stresses and the maximum depth and width of breakouts. The curves correspond to various values of φ_b, the half width, where $\mu = 0.6$ and $\Delta P = 0$ /after Zoback et al. 1985/.*

Stress magnitudes

The theory can be applied for the broad flat-bottomed breakouts observed in boreholes KFM01A and KFM01B. The corresponding figure but with a more realistic value of the coefficient of sliding for the Forsmark site, $\mu = 1.4$, is displayed in Figure 6-4. The average σ_H/σ_h-ratios of /Ask 2007/ for hydraulic data, overcoring data, joint solution with known elastic parameters, and joint solution with unknown elastic parameters yielded $\sigma_H/\sigma_h = 1.9$, $\sigma_H/\sigma_h = 1.7$, $\sigma_H/\sigma_h = 2.1$, $\sigma_H/\sigma_h = 1.5$, respectively. Using these ratios implies that breakouts that are 0.5, 1.0, and 1.5 mm deep have total widths of about 50–60°, 72–90°, and 90–110°, respectively. Unfortunately, the implications from Figure 6-4 cannot be verified with measured breakout depths with the currently available version of the WellCad program (WellCad reader). Instead the anticipated failure depth, r_b (calculated from the centre of the borehole, see Figure 6-2) was evaluated further for realistic values of the coefficient of sliding, stress ratio, and observed width of the breakout: the σ_H/σ_h-ratio was varied between 1.4 and 2.6, the internal friction angle between 50 and 60°, i.e. μ was varied between 1.2 and 1.7, and the breakout width was varied between 60 and 80°. The results are displayed in Table 6-1 and indicate that variations of the parameters within the chosen limits do not significantly affect the failure depth. For the stress ratio between 1.5 and 2.1 mentioned above, the failure depth outside the nominal borehole radius of 38 mm varies between 0.3–1.5 mm. For all parameter variations, the failure depth outside the nominal borehole radius varies between 0.3–1.8 mm.

Table 6-1. Calculation of r_b for various breakout widths, coefficients of sliding, and stress ratios.

φ_b [°]	μ [–]	σ_H/σ_h [–]	r_b [mm]	φ_b [°]	μ [–]	σ_H/σ_h [–]	r_b [mm]	φ_b [°]	μ [–]	σ_H/σ_h [–]	r_b [mm]
30	1.2	1.4	38.3	35	1.2	1.4	38.5	40	1.2	1.4	38.6
		1.6	38.5			1.6	38.7			1.6	38.9
		1.8	38.8			1.8	39.1			1.8	39.3
		2.0	38.9			2.0	39.2			2.0	39.5
		2.2	38.9			2.2	39.2			2.2	39.6
		2.4	39.0			2.4	39.3			2.4	39.7
		2.6	39.0			2.6	39.4			2.6	39.8
	1.4	1.4	38.3		1.4	1.4	38.4		1.4	1.4	38.4
		1.6	38.4			1.6	38.6			1.6	38.7
		1.8	38.6			1.8	38.8			1.8	39.0
		2.0	38.7			2.0	38.9			2.0	39.1
		2.2	38.7			2.2	39.0			2.2	39.2
		2.4	38.8			2.4	39.0			2.4	39.3
		2.6	38.8			2.6	39.1			2.6	39.4
	1.7	1.4	38.2		1.7	1.4	38.3		1.7	1.4	38.3
		1.6	38.3			1.6	38.4			1.6	38.5
		1.8	38.5			1.8	38.6			1.8	38.8
		2.0	38.5			2.0	38.7			2.0	38.8
		2.2	38.5			2.2	38.7			2.2	38.9
		2.4	38.6			2.4	38.8			2.4	39.0
		2.6	38.6			2.6	38.8			2.6	39.0

The breakout depth corresponds to r_b minus the borehole radius of 38 mm.

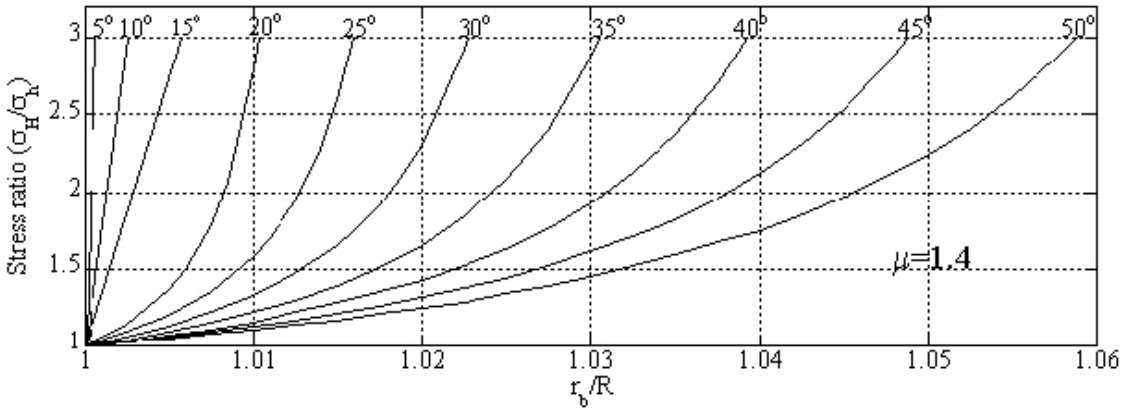

Figure 6 4. *Relationship between the ratio of the horizontal principal stresses and the maximum depth and width of breakouts. The curves correspond to various values of φ_b, the half width, where μ = 1.4 and ΔP = 0 /after Zoback et al. 1985/.*

The stress magnitudes may also be constrained using Equations (17) and (18) if the rock cohesive strength can be estimated. The cohesive strength is expressed by the relationship:

$$C = \frac{\sigma_{ci} \cdot (1 - \sin\varphi)}{2 \cdot \cos\varphi} \tag{20}$$

where σ_{ci} is the crack initiation strength (120 MPa; /SKB 2005/) and φ is the internal friction angle. The anticipated horizontal stresses were evaluated for observed breakout widths, realistic values of the coefficient of sliding, and breakout failure depth: the breakout width was varied between 60 and 80°, the breakout failure depth was set to 0.5 and 1.0 mm, and the internal friction angle was varied between 50 and 60° (expressed as different values of C in Table 6-2). The results are displayed in Table 6-2 and indicate that, assuming the stress profile of /Ask 2007/ based on hydraulic stress data, breakouts with a failure depth of 0.5 and 1.0 mm are anticipated from about 800 m (but 500 m for overcoring data). However, it should be noted that the results are strongly dependent upon the chosen stress profile by /Ask 2007/, which is only approximate. Moreover, a reduction of the crack initiation strength of 20% implies that the breakouts would appear below 500 m depth. Furthermore, the theory outlined above is based on that the excessive fluid pressure in the borehole is the same as that in the formation, i.e. ΔP = 0. /Zoback et al. 1985/ showed that ΔP strongly influences breakout development, where positive ΔP increases the normal stresses on potential failure planes near the borehole wall and inhibits failure, whereas negative ΔP lowers normal stresses and promotes failure.

Table 6-2. Calculation of horizontal stress magnitudes for various breakout widths, breakout failure depth, and cohesive strength (or coefficients of sliding).

φ_b [°]	r_b/R [–]	C [MPa]	σ_H [MPa]	σ_h [MPa]	φ_b [°]	r_b/R [–]	C [MPa]	σ_H [MPa]	σ_h [MPa]	φ_b [°]	r_b/R [–]	C [MPa]	σ_H [MPa]	σ_h [MPa]
30	1.013	16.1	60.0	30.5	35	1.013	16.1	63.5	41.3	40	1.013	16.1	65.7	48.2
		18.9	60.0	39.3			18.9	62.5	46.9			18.9	64.0	51.7
		21.8	60.0	44.6			21.8	61.8	50.3			21.8	63.0	53.8
	1.026	16.1	–	–		1.026	16.1	–	–		1.026	16.1	74.8	29.5
		18.9	–	–			18.9	65.9	28.7			18.9	69.5	40.3
		21.8	60.0	24.3			21.8	64.2	37.6			21.8	66.8	46.0

"–" implies that the stress ratio exceeds 3 and were excluded.

6.1.2 Deep borehole breakouts

Application of empirical method for horizontal stress magnitudes

Because the present analysis is conducted with a WellCAD Reader and not a full version of the WellCAD software, the collection of key data is troublesome and time consuming. As a result, the analysis only involves the most pronounced parts of the breakouts, which were analyzed every 0.1 m (Table 6-3). We emphasize that the depth estimates are only approximate and likely overestimated (only the maximum anomaly can be determined). This defeat aside, the results for these examples indicate that the average breakout failure depth and width are 5.5 mm and 60°, respectively (range 1–17 mm and 22–104°), and that σ_H is oriented about 130°N (125–135°N). However, the width of the breakout may be underestimated because it is difficult to pinpoint the breakout zone with the current WellCAD software (WellCAD Reader). It is judged that, based on all observed breakouts in both KFM01A and KFM01B, the breakout width is up to 90°.

Table 6-3. Detailed characterisation of breakouts in borehole KFM01B.

Bh length	R	r_b		α		φ_b		Breakout type
[mbl]	[m]	[m]		[°]		[°]		[–]
217.7	0.038	–	0.041	–	212	–	24	Diametrical
217.8	0.038	0.043	0.041	40	213	35	27	Diametrical
Average		0.042		35		29		
Range		0.041–0.043		32–40		24–35		
433.1	0.038	0.039*	–	41	–	11	–	Diametrical
433.2	0.038	0.042	–	35	–	33	–	Diametrical
433.3	0.038	0.039*	0.039*	36	231	29	23	Diametrical
433.4	0.038	0.049*	0.039*	36	204	32	12	Diametrical
433.5	0.038	0.051*	0.055*	45	220	52	35	Diametrical
433.6	0.038	0.051*	0.055*	55	223	45	40	Diametrical
433.7	0.038	0.044*	0.047	50	243	43	28	Diametrical
433.8	0.038	0.045	0.042*	47	237	33	31	Diametrical
433.9	0.038	0.043	0.043	51	220	42	30	Diametrical
434.0	0.038	–	0.039	–	241	–	25	Diametrical
434.1	0.038	–	0.043	–	208	–	22	Diametrical
434.2	0.038	0.039	–	38	–	12	–	Diametrical
434.3	0.038	–	0.039	–	242	–	18	Diametrical
Average		0.046		45		30		
Range		0.039–0.055		24–63		11–52		
463.9	0.038	0.041*	0.043	44	216	42	26	Diametrical
464.0	0.038	0.041*	0.042	45	210	40	25	Diametrical
Average		0.042		39		33		
Range		0.041–0.043		30–45		25–42		

"*" and "–" denote somewhat uncertain estimates and not measurable estimates, respectively (with currently available WellCAD software).

The empirical method by /Martin et al. 1999/, based on case studies of excavations around the world failing in a progressive and non-violent manner, expresses the relationship between the depth of failure, r_b, and stress magnitude. Their studies showed that the depth of failure normalized with the tunnel radius, a, is linearly proportional to the stress level σ_{max}/σ_c, calculated as the ratio of maximum tangential stress at the wall of a circular opening to the laboratory uniaxial compressive strength, σ_c:

$$\frac{r_b}{R} = 1.25 \cdot \frac{\sigma_{\max}}{\sigma_c} - 0.5 \pm 0.1 \quad (21)$$

or reformulated

$$\sigma_{\max} = \frac{\sigma_c \cdot r_b}{1.25 \cdot R} + 0.5 \pm 0.1 \quad (22)$$

The uniaxial compressive strength was for borehole KFM01A determined to 225 ± 22 MPa /SKB 2005/. These results, together with data in Table 6-3, can then be used to predict the maximum tangential stress. The results imply (Table 6-4) that σ_c ranges between 159 and 291 MPa when varying breakout failure depth (A, B and C correspond to min, average and max failure depth from Table 6-3, respectively) and varying σ_c within a 99% confidence interval. For comparison, also the crack in initiation strength of 120 MPa /SKB 2005/ was used in the calculations.

Assuming that the formation pore pressure can be neglected, the maximum tangential stress can be expressed as:

$$\sigma_{\max} = 3 \cdot \sigma_H - \sigma_h \quad (23)$$

As noted previously, /Ask 2007/ estimated the horizontal stresses at Forsmark based on four different approaches: (i) hydraulic stress data (σ_h = 16.9+0.035 (z-560) MPa and σ_H = 32.3+0.104 (z-560) MPa); (ii) overcoring stress data (σ_h = 17.5+0.036 (z-250) MPa and σ_H = 30.5+0.074 (z-250) MPa); (iii) joint solution of hydraulic and overcoring data with known eleastic parameters (σ_h = 19.1+0.013 (z-500) MPa and σ_H = 40.1+0.060 (z-500) MPa), and (iv) joint solution of hydraulic and overcoring data with unknown eleastic parameters (σ_h = 16.8+0.021 (z-500) MPa and σ_H = 26.4+0.042 (z-500) MPa; /Ask 2007/. In the following, we use two cases, the solution that results in minimum respectively maximum tangential stress at the depth of the breakouts.

Table 6-4. Prediction of maximum tangential stress, σ_{max}, for pronounced breakouts.

Breakout depth [mbl]	σ_c [MPa]	α [m]	r_b A [m]	r_b B [m]	r_b C [m]	σ_{max} A [MPa]	σ_{max} B [MPa]	σ_{max} C [MPa]
217	120	0.038	0.041	0.042	0.043	103.5±0.1	106.1±0.1	108.6±0.1
	159	0.038	0.041	0.042	0.043	137.7±0.1	141.1±0.1	144.4±0.1
	225	0.038	0.041	0.042	0.043	194.7±0.1	199.4±0.1	204.2±0.1
	291	0.038	0.041	0.042	0.043	251.7±0.1	257.8±0.1	263.9±0.1
433	120	0.038	0.039	0.046	0.055	98.5±0.1	116.2±0.1	138.9±0.1
	159	0.038	0.039	0.046	0.055	131.0±0.1	154.5±0.1	184.6±0.1
	225	0.038	0.039	0.046	0.055	185.2±0.1	218.4±0.1	261.0±0.1
	291	0.038	0.039	0.046	0.055	239.4±0.1	282.3±0.1	337.4±0.1
464	120	0.038	0.041	0.042	0.043	103.5±0.1	106.1±0.1	108.6±0.1
	159	0.038	0.041	0.042	0.043	137.7±0.1	141.1±0.1	144.4±0.1
	225	0.038	0.041	0.042	0.043	194.7±0.1	199.4±0.1	204.2±0.1
	291	0.038	0.041	0.042	0.043	251.7±0.1	257.8±0.1	263.9±0.1

The result for $\sigma_{h,measured}$ from the different solutions may be used to calculate maximum horizontal stress from the borehole breakout data ($\sigma_{H,BB}$), which can be compared with the corresponding value of σ_H from the different solutions ($\sigma_{H,measured}$; Table 6-5).

The results indicate that the magnitudes of $\sigma_{H,BB}$ are generally considerably larger than those of $\sigma_{H,Hydr}$. The breakout at 217 m depth cannot be explained by any stress profile, whereas the breakouts at 433 and 464 may be explained by the overcoring data and minimum material strength (corresponding to crack initiation). Because most breakouts in the investigated boreholes have a very limited failure depth and that deeper breakouts are only observed locally, this may be explained by that the more pronounced breakouts coincide with zones of reduced compressive strength and/or high-stress zones. On the other hand, most stress profiles could explain the breakouts with only minor variations.

The empirical method of /Martin et al. 1999/ may also be presented graphically to evaluate at what depth range breakouts of given failure depths may be anticipated. In Figure 6-5, the compressive strength, σ_c, versus depth is displayed where σ_c was calculated for observed breakout failure depths and tangential stress based on hydraulic stress data by /Ask 2007/. The result indicates that continuous breakouts above 1,000 m would not appear in sound rock corresponding to the average compressive strength (225 MPa). However, breakouts with small failure depths (0.5–2 mm) would appear from about 550 mvd (metres vertical depth) using the lower limit of the compressive strength (159 MPa). If the compressive strength is further reduced to the crack initiation strength, these would start to appear about 300 mvd. Thus, this may possibly explain why most observed breakouts have very limited failure depths, whereas a low-amplitude pattern on two diametrically opposite sides of the borehole is clearly visible, i.e. they may be premature breakouts. If so, these breakouts will grow in depth with time, whereas the width is left more or less unaffected /Zoback et al. 1985/. However, the observed breakouts above 300 m depth cannot be explained by this theory. We emphasize again that the implications outlined above are strongly dependent upon the chosen approximate hydraulic stress profile by /Ask 2007/ and on pore pressure effects (which were assumed negligible). Moreover, it has been assumed that the boreholes are vertical and parallel with a principal stress direction.

Table 6-5. Prediction of maximum horizontal stress from deep borehole breakouts, $\sigma_{H,BB}$.

Depth	σ_{max}			$\sigma_{h,measured}$		$\sigma_{H,BB}$						$\sigma_{H,measured}$	
[mbl]	A	B	C			A		B		C			
	[MPa]	[MPa]	[MPa]	[MPa]		[MPa]		[MPa]		[MPa]		[MPa]	
				Min	Max	Min	Max	Min	Max	Min	Max	Min	Max
217	103.5	106.1	108.6	10.8[1]	16.3[3]	38.1	39.9	39.0	40.8	39.8	41.6	14.6[1]	28.1[3]
	137.7	141.1	144.4	10.8[1]	16.3[3]	49.5	51.3	50.6	52.5	51.7	53.6	14.6[1]	28.1[3]
	194.7	199.4	204.2	10.8[1]	16.3[3]	68.5	70.3	70.1	71.9	71.7	73.5	14.6[1]	28.1[3]
	251.7	257.8	263.9	10.8[1]	16.3[3]	87.5	89.3	89.5	91.4	91.6	93.4	14.6[1]	28.1[3]
433	98.5	116.2	138.9	12.5[2]	24.1[3]	37.0	40.9	42.9	46.8	50.5	54.3	19.1[2]	44.0[3]
	131.0	154.5	184.6	12.5[2]	24.1[3]	47.8	51.7	55.7	59.5	65.7	69.6	19.1[2]	44.0[3]
	185.2	218.4	261.0	12.5[2]	24.1[3]	65.9	69.8	77.0	80.8	91.2	95.0	19.1[2]	44.0[3]
	239.4	282.3	337.4	12.5[2]	24.1[3]	84.0	87.8	98.3	102.1	116.6	120.5	19.1[2]	44.0[3]
464	103.5	106.1	108.6	13.5[2]	25.2[3]	39.0	42.9	39.9	43.8	40.7	44.6	22.3[2]	46.3[3]
	137.7	141.1	144.4	13.5[2]	25.2[3]	50.4	54.3	51.5	55.4	52.6	56.5	22.3[2]	46.3[3]
	194.7	199.4	204.2	13.5[2]	25.2[3]	69.4	73.3	71.0	74.9	72.6	76.5	22.3[2]	46.3[3]
	251.7	257.8	263.9	13.5[2]	25.2[3]	88.4	92.3	90.4	94.3	92.5	96.4	22.3[2]	46.3[3]

Note: [1] denotes joint solution with unknown elastic parameters; [2] denotes hydraulic solution; and [3] denotes overcoring solution.

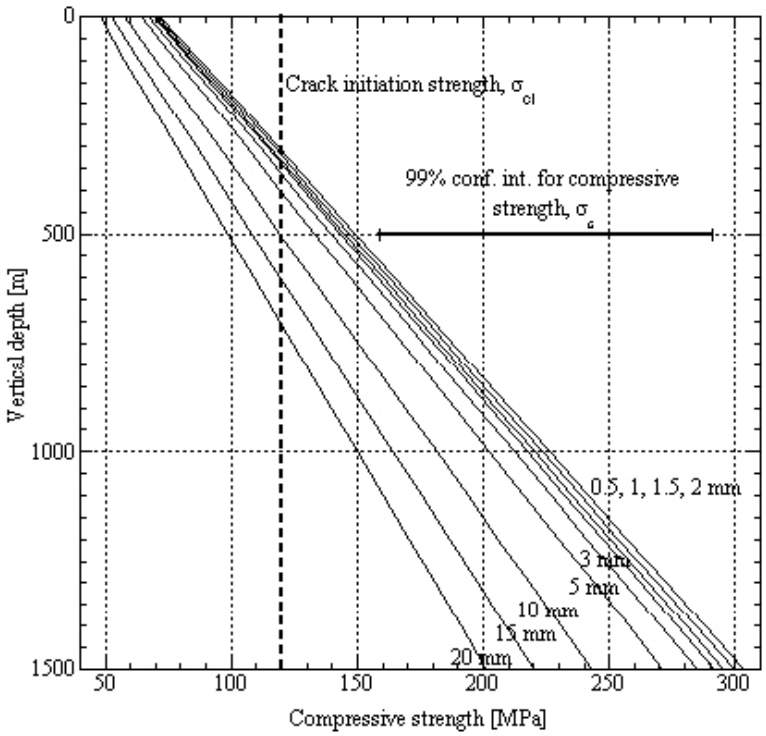

Figure 6-5. *The compressive strength as a function of depth when using the stress profile by /Ask 2007/ based on hydraulic stress data.*

6.1.3 Effect of drilling

An explanation to the suggested frequent occurring breakouts indicated by the BHTV may be influence of drilling. The experience from drilling differs significantly between the Oskarshamn and Forsmark investigation sites. In Forsmark, the dominant rock type in the investigated boreholes is a metagranite with a quartz content ranging 20–45% /SKB 2005/, which is about 20% larger compared with the Oskarshamn site /Askling and Odén 2004/. The experience from core drilling is that the rock is very hard. The drill bit wear is larger and the feed force is up to 30% higher than at similar depths in Oskarshamn. Despite of greater feed force, the drill rate is significantly lower at Forsmark (~9–13 cm/min) compared with that at Oskarshamn (~12–18 cm/min). The flush water pressure at Forsmark is also higher compared with the Oskarshamn site as a result of that the spacing between drillpipe and borehole is smaller (the flush water flow is 30–35 l/min at both sites). The higher feed force and the lower drill rate in Forsmark result in a higher friction at the rock-drill bit contact, which leads to increases in rock temperature, heat expansion, and induced thermal stress of the rock. The impact of this transient, 3D thermo-mechanical effect is not fully understood /Ask et al. 2006/.

Perhaps the most pronounced evidence of the drilling effect on breakout development is displayed on amplitude logs during various drilling stops. In Figure 6-6, drilling is stopped at about 470.6 mbl in borehole KFM01B. Prior to drilling stop, the grain-sized breakouts are relatively pronounced, whereas the continued drilling displays considerably less developed breakouts. We interpret this to be a result of primarily drilling temperature. Due to the high content of quartz at the Forsmark site, it is conceivable that the normal drilling temperature is elevated compared to sites with smaller content of quartz. However, when the drilling is put to a halt, the temperature in the well decreases and will, if the stop endures long enough, return to the in situ temperature in the bedrock at present depth. As the drilling subsequently is continued, the temperature will once again increase, leading to progressively more pronounced breakouts.

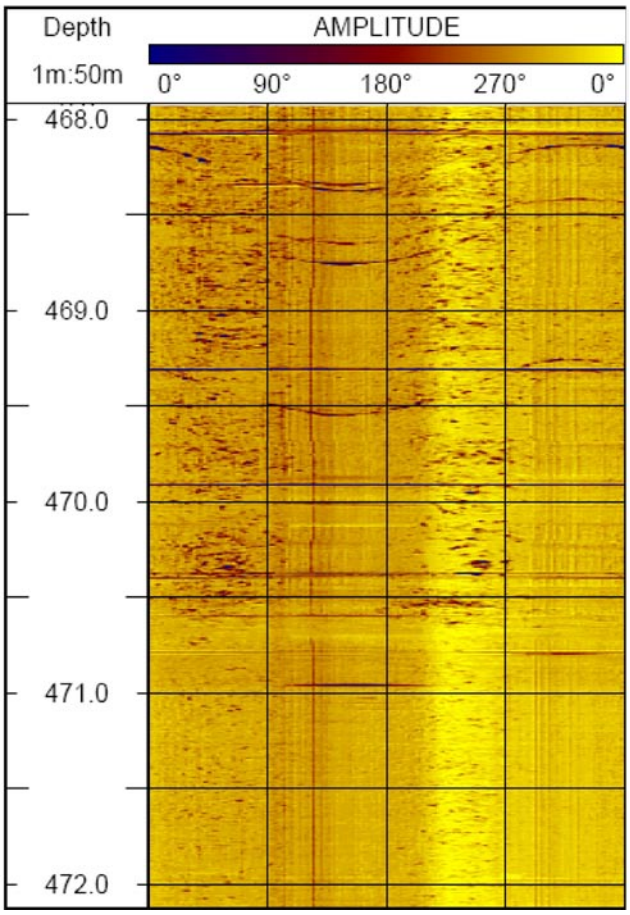

Figure 6-6. *The amplitude log displays a sharp border at c 470.6 mbl between relatively pronounced and moderate grain-sized breakouts, which coincide with a drilling stop in borehole KFM01B. Hence, breakout development is clearly linked to drilling.*

6.2 Potential drilling-induced fractures

In borehole KFM01B, features that resemble drilling induced fractures (DIFs) were identified, see Figure 5-18. If this would indeed be true DIFs, they would require low tangential stresses in the direction of maximum horizontal stress. However, none of the stress profiles by /Ask 2007/ may explain drilling induced fractures.

6.3 Uncertainties in existing data

6.3.1 Measurement accuracy of the BTHV

The axial and vertical resolution depends on the frequency of the transmitted pulse and the speed of logging, respectively. For example, the logging speed applied in boreholes KFM01A and KFM01B were 2.0–2.4 m/h and the reported vertical resolution 2 mm /Nielsen and Ringgaard 2003, 2004/. /Nielsen and Ringgaard 2003/ specified that the vertical sampling interval was 2 mm in borehole KFM01A, implying that the maximum transducer frequency of 20 revolutions per second was used during logging. The transducer frequency of 1.5 MHz corresponds to a wavelength of 0.7 µm, but the accuracy is lower than 0.7 µm as a result of the combined effects of logging speed, rotation-rate of the mirror, transducer frequency, as well as of the centralization of tool within the borehole, and of the types of processing that are applied to the data. In a recent study, Håkan Mattsson (pers. comm. 2006) suggests that the radial resolution of the data from boreholes KFM01A and KFM01B is at least ± 0.2 mm.

6.3.2 Centralization of the tool

The limitation of the BHTV tool is associated with the fact that the tool emits and receives ultrasonic pulses. It is essential that the tool be centralized in the borehole, because the emitted pulses are not reflected back to the tool if it is off-centre. Moreover, particles in the borehole fluid scatter and prevent part of the pulse from reflecting at the borehole wall. Finally, the results are depending on acoustic contrasts at the borehole wall. Fractures, voids, soft material, as well as borehole breakouts and drilling-induced fractures (DIFs) absorb or scatter much of the pulse, which produces low-amplitude and high travel time reflectance or dark zones in the unwrapped images.

A non-centralized tool results in erroneous mean caliper readings, where maximum and minimum caliper readings over- and underestimate the true borehole radius. In inclined boreholes, maximum and minimum caliper readings appear on the upper (hanging wall) and lower (foot wall) sides of the borehole, respectively. To investigate if the tool was properly centralized, a 200 m section (100–300 mbl) in borehole KFM01B was investigated every 10 m. The results indicate that the average maximum and minimum radiuses are 77.3 and 73.6 mm, respectively. The maximum reading is in average oriented 280°N and minimum reading 84°N. These directions nearly coincide with the orientation of the hanging and foot walls of the borehole (272°N and 92°N, respectively) but the directions are too scattered to be conclusive. However, based on the 3D-caliper data, the crude investigation entails that there is a centralization problem between 100–300 mbl in borehole KFM01B.

We suggest that the centralization aspect is investigated further.

6.3.3 Length calibration error

The available data have posed certain questions regarding the way data handling was conducted. For example, the sections explaining the length calibration of the BHTV /Nielsen and Ringgaard 2003, 2004/ are confusing. It became clear that although e.g. the high-resolution 3D-caliper was correctly calibrated, the summary plots (e.g. Figure 5-1), from which the figures in this report were taken, have a length error. However, the plots showing the borehole seen from above using the high-resolution 3D-caliper, e.g. Figure 5-3, are correctly length calibrated. For the next stage, in order to minimize such errors, we need additional information about the BHTV logging and the tool itself.

6.3.4 Temperature effects

During this study, it has come to our knowledge that the BHTV data have not been calibrated with respect to temperature. However, we do not consider this a major source of uncertainty and it primarily affects the measurement of breakout failure depth. Thus, this temperature shortcoming, as well as the uncertainty in the mean caliper reading (±0.5 mm) used to determine the breakout failure depth, will probably result in small uncertainties in the stress magnitudes but they will most likely be considerably less than uncertainties related to the imprecise measures of compressional strength. For this reason, breakout theory can only provide crude bounds of the stress magnitudes. However, for stress orientations and evaluation of the continuity of the stress field in a rock mass, it is one of the most successfully applied methods worldwide.

7 Recommendations for future research

Recommendation for future studies are made in two scales; the present scale involving Drill Site 1 and boreholes KFM01A and KFM01B, and a larger scale involving the entire Forsmark site.

7.1 Stress-induced elongations at the present scale – Drill Site 1

This initial study has demonstrated that large parts of boreholes KFM01A and KFM01B contain borehole breakouts, although their development is not fully understood in the present absence of reliable estimates of the prevailing stress magnitudes at the Forsmark site. In addition, there are indications that drilling-induced tensile fractures occur in borehole KFM01B. Consequently, our first recommendation is to launch the detailed study on stress-induced borehole elongations in these two boreholes, with the objective to characterize the state of horizontal stresses, i.e. their orientations and magnitudes.

WellCAD Reader has been a useful program for the initial analysis of borehole elongations in boreholes KFM01A and KFM01B. However, for detailed inspection of the data, it is necessary to make interactive interpretations on screen and to obtain computer generated result files with data such as failure depth, azimuth, width, etc of the selected breakout. It would also be useful if the colour scale of the azimuth and travel time images could be controlled: not only would this provide information on the size of the azimuth and travel time variation, but it would also allow alteration and highlighting of interesting sections of that scale (i.e. a dynamic colour scale rather than the present static colour scale). This is especially important for evaluating the differences between travel time and amplitude logs as described by /Deltombe and Schepers 2000/, who noted that the former gives the true fallout and the latter the wider damage zone. This has significant influence on the estimates of stress magnitudes as it determines if the crack initiation strength or the uniaxial compression strength should be used for the calculations (see Chapter 6). Although time has not permitted a detailed inspection of the full version of the WellCAD program, we suspect that these features, i.e. on-screen interpretation, automatic results file generation, and dynamic colour scale control, are available in the full WellCAD version. Our second recommendation, hence, is that the next stage in stress analyses should be using the full WellCAD program. Should our assumption be wrong, we would need access to such a program.

The detailed study on stress-induced borehole-elongation would follow the following steps:

1 Detailed mapping of borehole breakout orientation using an interactive computer program (probably full version of WellCAD, or other program) and obtaining result files with average breakout azimuth, failure depth, length.

2 Investigate effect of borehole inclination on borehole breakout orientation /e.g. Mastin 1988, Peska and Zoback 1995, Zoback et al. 2003/.

3 Classify the average borehole breakout occurrence individually and jointly for boreholes KFM01A and KFM01B, according to World Stress Map (WSM) ranking.

4 Detailed mapping of potential DIFs according to WSM ranking.

5 Identify potential decoupling zones.

6 Estimate stress magnitudes from borehole breakouts and the potential DIFs with existing theories. This will include detailed mapping of the individual width of borehole breakouts and DIFs (obtained in full version of WellCAD, or other program). Access to rock strength data routinely collected by SKB is necessary. Additional rock strength measurements may however be required. If the study on borehole breakout width is providing unsatisfactory

results, we will further characterize the borehole breakouts and attempt to estimate the horizontal stress magnitudes using borehole shape /e.g. Guenot 1987, Maury and Sauzay 1987/.

7 Compare the results with existing stress data.

The available data have posed certain questions regarding the way data handling was conducted and later processed. The most important questions include: (1) what equipment type was actually used during logging and as the tool specifications differ from those of he manufacturers – all dimensions are required; (2) what was the frequency of the ultrasonic pulse and the axial resolution of the signal; (3) why were two different logging speeds used in the boreholes – as detailed data as possible of it's variation downhole is required; (4) what is the downhole variation in torque in the logging cable; (5) why were centralizing springs only used in KFM01B and not in KFM01A although both boreholes deviate from the vertical, and what is the location and capacity of the centralizing springs; (5) what is the location and capacity of the piezoelectric transducer; (6) what configuration was used during logging with respect to other logging tools run together with the BHTV; (7) are there repeated logging sections available; (8) how was the length calibration made; and (9) how big is the temperature effect. To this, we also need the Daily report from logging as well as the temperature and resistivity data logs from the data of the BHTV logging.

Once these questions have been resolved and the detailed characterization of stress-induced elongations has been completed for Drill Site 1, our third recommendation is to enlarge the study to the Forsmark site scale, which is outlined below.

7.2 Stress-induced elongations at the Forsmark site scale

The state of stress at the Forsmark site has proven to be one of the most important issues regarding the potential of the site for a future repository of nuclear waste. To describe the benefits of data from stress-induced elongations compared with point-wise stress measuring techniques such as overcoring and hydraulic methods, it is necessary to first outline the concept of stress.

The concept of stress is a concept of continuum mechanics. It applies only in bodies that are regular enough to be approximated by a continuum. Because the stress at a point involves six components, the determination of the regional stress field includes determination of six functions for the domain under consideration. When using point-wise stress measuring techniques, this requires integration of measurements conducted at points that sample properly the continuum volume of interest.

Thus, prior to discussing how to ascertain the validity of a specific stress measurement at a certain point, it is necessary to identify volumes where the continuity hypothesis is verified. It is completely pointless to compare a single stress measurement at a given depth with that at another depth if the two points of measurements do not belong to the same continuum. This is one of the major difficulties in crystalline rocks and only preliminary geological and geophysical reconnaissance can help answer this question /Ask and Cornet 2006/.

A crucial point that has been missing so far in the attempts to determine the regional stress field at the Forsmark site is an evaluation of the continuity hypothesis. In this respect, data from stress-induced elongations are extremely valuable because continuous information along a borehole is collected, which can be used to pinpoint decoupling zones in the rock. Because decoupling zones may exist, identifying these and determining their effect on the stress field is an important objective.

We strongly recommend that breakout analysis in the boreholes penetrating and surrounding the rock volume of the planned repository is conducted. These results, together with a careful analysis of cores and other geophysical data would effectively resolve the continuity aspect at the site. Once completed, the results may be used for selecting points of future stress measurements and for selecting the set of data that will be used for the regional stress evaluation.

8 References

Aaltonen J, Gustafsson C, 2003. RAMAC and BIPS logging in borehole KFM01A. SKB P-03-45, Svensk Kärnbränslehantering AB.

Amadei B, Stephansson O, 1997. Rock Stress and Its Measurements, Chapman and Hall Publ., London.

Ask M V S, 1998. In-situ and laboratory stress investigations using borehole data from the North Atlantic Ocean. Doctoral Thesis, Royal Institute of Technology, Stockholm.

Ask D, Cornet FH, 2006. Risk assessment of hydraulic stress measurements at Forsmark. SKB Internal report.

Ask M V S, Ask D, Christiansson R, 2006. Detection of borehole breakouts at the Forsmark site. Proc. Int. Symp. on In-Situ rock stress, Trondheim, Norway, pp. 79–86.

Ask D, 2007. Evaluation of hydraulic and overcoring stress measurements in boreholes KFM01A, KFM01B, KFM02A, and KFM04A at the Forsmark site. SKB P-07-234, Svensk Kärnbränslehantering AB.

Askling P, Odén A, 2004. Svarvning av borrkärna och borrhålsvägg samt uppkomst av spiralmärken vid kärnborrning. SKB PIR-04-02, Svensk Kärnbränslehantering AB.

Barton C A, Zoback M D, Burns K L, 1988. In-situ stress orientation and magnitude at the Fenton geothermal site, New Mexico, determined from wellbore breakouts. Geophys. Res. Lett., 15, pp. 467–70.

Bell JS, Gough DI, 1979. Nortwest-southeast compressive stress in Alberta: Evidence from oil wells. Earth Plant. Sci. Lett., 45, pp. 475–82.

Berard T, Cornet FH, 2002. Borehole breakouts and focal mechanisms analysis in deep geothermal wells. In Proc. North Am. Rock Mech. Symp., NARMS_TAC, Toronto, Canada (Eds. Hammah et al.), pp. 1341–6. A.A Balkema: Rotterdam.

Berglund J, Petersson J, Wängnerud A, Danielsson P, 2004. Boremap mapping of core drilled borehole KFM01B. SKB P-04-114, Svensk Kärnbränslehantering AB.

Brudy M, Zoback MD, 1993. Compressive and tensile failure of boreholes arbitrary inclined to principal stress axis: application to the KTB boreholes, Germany. Int. J. Rock. Mech. Min. Sci., 30, pp. 1035–8.

Deltombe J-L, Schepers R, 2000. Combined Processing of BHTV Traveltime and Amplitude Images. In Proc. Int. Symp. Borehole Geophysics for Minerals, Geotechnical, and Groundwater applications, Golden, CO, United State, Vol. 7, pp. 29–42.

Engelder T, 1993. Stress regimes in the lithosphere, Princeton University Press: Princeton, New Jersey.

Gough D I, Bell J S, 1981. Stress orientations from oil-well fractures in Alberta and Texas. Can. J. Earth Sci., 20, pp. 638–45.

Guenot A, 1987. Stress and rupture concentrations around oil wellbores. In Proc. 6th Int. Congr. Rock Mech., Montreal, Canada (Eds. Herget G, Vongpaisal S), pp. 109–18. A.A Balkema: Rotterdam, Boston.

Gustafsson J, Gustafsson C, 2004. RAMAC and BIPS logging in borehole KFM01B and RAMAC directional re-logging in borehole KFM01A. SKB P-04-79, Svensk Kärnbränslehantering AB.

Haimson B C, Song I, 1993. A laboratory study of borehole breakouts in Cordova Cream: A case of shear failure mechanism. Int. J. Rock. Mech. Min. Sci., 30, pp. 1047–56.

Jaeger J C, Cook N G W, 1969. Fundamentals of rock mechanics. Chapman and Hall Ltd and Science Paperbacks, London.

Kirsch G, 1898. Die Theorie der Elastizität und die Bedürfnisse der Festigkeitslehre. Zeit Ver. Dt. Ingenieure, 42, pp. 797–807.

Klee G, Rummel F, 2004. Rock stress measurements with hydraulic fracturing and hydraulic testing of pre-existing fractures in borehole nos. KFM01A, KFM01B, KFM02A and KFM04A. Results of in-situ tests. SKB P-04-311, Svensk Kärnbränslehantering AB.

Lindfors U, Perman F, Sjöberg J, 2004. Evaluation of overcoring results from KFM01B. SKB P-05-66, Svensk Kärnbränslehantering AB.

Loberg B, 1999. Geologi. Material, processer och Sveriges berggrund, 6th edition. Prisma, Stockholm.

McClintock F A, Walsh J B, 1962. Friction on Griffith cracks under pressure. In Proc. 4th U.S. Natl. Congr. Appl. Mech., pp. 1015–21.

Martin C D, Kaiser P K, McCreath D R, 1999. Hoek-Brown parameters for predicting the depth of brittle failure around tunnels. Can. Geotech. J., 36(1), pp. 136–51.

Mastin L, 1988. Effect of borehole deviation on breakout orientations. J. Geohys. Res., 93, p. 9187–95.

Maury V, Sauzay J-M, 1987. Borehole instability: case histories, rock mechanics approach and result. In: Proc. SPE/IADC drilling conf. New Orleans March 15–18, SPE 16051.

Maury V, Etchecopar A, Pezard P A, 1999. New borehole imagery techniques: an aid for failure modes and in-situ stress analysis and for minimizing drilling incidents. SPWLA Transactions 1999, Oslo, Norway.

Moos D, Zoback M D, 1990. Utilization of observations of well bore failure to constrain the orientation and magnitude of crustal stresses: Application of continental, Deep Sea Project and Ocean Drilling Program boreholes. J. Geohys. Res., 95, pp. 9305–25.

Nielsen U T, Ringgaard J, 2003. Geophysical borehole logging in borehole KFM01A, HFM01 and HFM02. SKB P-03-103, Svensk Kärnbränslehantering AB.

Nielsen U T, Ringgaard J, 2004. Geophysical borehole logging in borehole KFM01B, HFM14, HFM15, HFM16, HFM17, and HFM18. SKB P-04-145, Svensk Kärnbränslehantering AB.

Peska P, Zoback M D, 1995. Compressive and tensile failure of inclined well bores and determination of in situ stress and rock strength. J. Geohys. Res., 100, pp. 12791–811.

Petersson J, Wängnerud A, 2003. Boremap mapping of telescope drilled borehole KFM01A. SKB P-03-23, Svensk Kärnbränslehantering AB.

Plumb R A, Hickman S H, 1985. Stress-induced borehole elongation: A comparison between four-arm dipmeter and the borehole televiewer in the Auburn geothermal well. J. Geophys. Res., 90, pp. 5513–21.

Plumb R A, 1989. Fracture patterns associated with incipient borehole breakouts. In Rock at great depth (Eds. Maury V, Fourmaintaux D), 2, pp. 761–8. A.A Balkema, Rotterdam.

Reinecker J, Heidbach O, Tingay M, Conolly P, Mueller B, 2004. The 2004 release of the World Stress Map (available online at www.world-stress-map.org).

Sjöberg J, 2004. Overcoring rock stress measurements in borehole KFM01B. SKB P-04-83, Svensk Kärnbränslehantering AB.

Sjöberg J, Lindfors U, Perman F, Ask D, 2005. Evaluation of the state of stress at the Forsmark site. Preliminary site investigation Forsmark area. SKB R-05-35, Svensk Kärnbränslehantering AB.

SKB, 2005. Preliminary site description. Forsmark area – version 1.2. SKB R-05-18, Svensk Kärnbränslehantering AB.

Zajac B J, Stock J M, 1997. Using borehole breakouts to constrain the complete stress tensor: Results from the Siljan Deep Drilling Project and offshore Santa Maria Basin, California. J. Geophys. Res., 102, pp. 10083–100.

Zheng Z, Cook N G W, Mastin L, Andersson R N, 1988. Borehole breakouts and stress measurements. In Key questions in Rock Mechanics (Eds. Cunsall PA, Sterling RL, Starfield AM), pp. 471–8. A.A Balkema, Rotterdam.

Zoback M D, Moos D, Mastin L, Andersson R N, 1985. Borehole breakouts and in-situ stress. J. Geophys. Res., 90, pp. 5523–30.

Zoback M D, Barton C A, Brudy M, Castillo D A, Finkbeiner T, Grollimund B R, Moos D B, Peska P, Ward C D, Wiprut D J, 2003. Determination of stress orientation and magnitude in deep wells. Int. J. Rock. Mech. Min. Sci., 40, pp. 1049–76.

Appendix 1

Identified breakouts in borehole KFM01A

Table A1-1. Positively identified and potential stress-induced borehole breakouts in borehole KFM01A and rough estimate of σ_H-orientation.

Depth section [mbl]	Orientation σ_H [°N]	Type of BB	Degree of clarity	Rock type
111.8–119.0	NNW-SSE	Diametrical	Low	G3
140.0–144.2	NW-SE	Diametrical	Medium	G3
174.0–179.0	NW-SE	Diametrical	Low	G3, A
215.0–217.0	NNW-SSE	Diametrical	Medium	G3
246.8–248.2	NNW-SSE	Diametrical	Medium	G3
267.4–268.2	NW-SE	Diametrical	Low	G3
352.0–358.5	NW-SE	Single	Low	G3
371.8–374.0	NNW-SSE	Diametrical	Low	G3
389.7–393.0	NNW-SSE	Diametrical	High	G3
406.9–408.5	NNW-SSE	Diametrical	Low	G3
428.0–432.0	NNW-SSE	Diametrical	Medium	G3
476.5–482.0	NNW-SSE	Diametrical	High	G3
486.5–493.0	NW-SE	Diametrical	Medium	G3
565.3–572.7	NW-SE	Diametrical	Low	G3
589.7–590.9	NW-SE	Diametrical	Low	G3
604.0–604.3	NW-SE	Diametrical	Medium	G3
607.7–610.5	NE-SE	Diametrical	Low	G3
610.8–613.3	NW-SE	Diametrical	High	G3
613.3–626.6	NW-SE	Diametrical	Low	G3
658.0–661.0	NW-SE	Diametrical	High	G3
728.5–737.2	NW-SE	Diametrical	Low	G3, A
742.0–745.2	NW-SE	Diametrical	Medium	G3
745.3–773.0	NW-SE	Diametrical	Medium to Low	G3, A, G1
776.0–778.0	NW-SE	Single	High	G3, G1
783.5–791.0	NNW-SSE	Diametrical	Low	G3, G1
792.0–809.0	NW-SE	Diametrical	Low to Medium	G3, G2
830.0–833.6	NNW-SSE	Diametrical	High	G2
834.0–848.0	NW-SE	Diametrical	Low to Medium	G2
852.0–854.0	NW-SE	Diametrical	Medium	G2
860.0–874.5	NW-SE	Diametrical	Low to Medium	G2, G3
885.0–957.0	NW-SE to NNW-SSE	Diametrical	Medium to High	G3, G2, G1
957.0–969.0	NW-SE to NNW-SSE	Diametrical	Medium	G3, G2
974.7–987.0	NW-SE to NNW-SSE	Diametrical	Medium to High	G2, G3
990.0–1,000.8	NW-SE to NNW-SSE	Diametrical	Medium to High	G3
Average	NW-SE			

Keys: G1 = Granite, fine- to medium-grained; P = Pegmatite, pegmatitic granite; G2 = Granite, granodiorite and tonalite, metamorphic, fine- to medium-grained; G3 = Granite to granodiorite, metamorphic, medium-grained; A = Amphibolite; CS = Calc-silicate rock (skarn). Note that the depths are not fully accurate.

Appendix 2

Identified breakouts in borehole KFM01B

Table A2-1. Positively identified and potential stress-induced borehole breakouts in borehole KFM01B and rough estimate of σ_H-orientation.

Depth section [mbl]	Orientation σ_H [°N]	Type of BB	Degree of clarity	Rock type
113.5–117.5	NNW-SSE	Diametrical	High	G3
120.0–124.2	NNW-SSE	Diametrical	High	G3
127.5–136.5	NNW-SSE	Diametrical	High	G3, A
139.5–142.4	NW-SE	Diametrical	Low	G3, P
142.5–153.0	NNW-SSE	Diametrical	Medium	P, G3
153.1–186.5	NW-SE	Diametrical	Medium	G3
186.8–188.9	NW-SE	Prim. single	High	G3
190.2–200.3	NNW-SSE	Diametrical	High	G3
202.9–204.2	NW-SE	Diametrical	High	G2
210.8–218.0	NW-SE	Diametrical	Low	G3
218.0–218.3	NW-SE	Diametrical	High	G3
218.4–224.5	NW-SE	Diametrical	Low	G3,G2
224.6–235.2	NW-SE	Diametrical	High	G3
239.0–246.0	NW-SE	Single, diam.	Low	G3
254.6–270.0	NW-SE	Single, diam.	Low	G3, G2
308.0–311.5	NNW-SSE	Diametrical	Medium	G3
373.8–374.3	NNW-SSE	Single, diam.	High	G3
377.1–378.1	NW-SE	Single	High	G3
383.0–386.2	NW-SE	Diametrical	Medium	G3
398.6–406.8	NW-SE	Diametrical	High	G3
430.8–439.0	NW-SE	Diametrical	High	G3
439.1–447.0	NW-SE	Single	Medium	G3
454.6–458.1	WNW-ESE	Diametrical	High	P, G3
462.8–464.5	NW-SE	Diametrical	High	G3
465.0–471.0	NW-SE	Diametrical	High	G3
471.1–481.9	NW-SE	Diametrical	Medium	G3
482.0–498.6	NW-SE	Diametrical	High	G3
Average	NW-SE			

Keys: G1 = Granite, fine- to medium-grained; P = Pegmatite, pegmatitic granite; G2 = Granite, granodiorite and tonalite, metamorphic, fine- to medium-grained; G3 = Granite to granodiorite, metamorphic, medium-grained; A = Amphibolite; CS = Calc-silicate rock (skarn). Note that the depths are not fully accurate.